Journal of Medicinal Chemistry

Article

Cite This: J. Med. Chem. 2019, 62, 3722−3740

pubs.acs.org/jmc

Dopamine D_4 Receptor-Selective Compounds Reveal Structure−Activity Relationships that Engender Agonist Efficacy

Thomas M. Keck,[†,‡,#] R. Benjamin Free,[⊥,#] Marilyn M. Day,[⊥] Sonvia L. Brown,[§] Michele S. Maddaluna,[§] Griffin Fountain,[†] Charles Cooper,[†] Brooke Fallon,[†] Matthew Holmes,[†] Christopher T. Stang,[⊥] Russell Burkhardt,[∥] Alessandro Bonifazi,[∥] Michael P. Ellenberger,[∥] Amy H. Newman,[∥] David R. Sibley,[⊥] Chun Wu,[†] and Comfort A. Boateng*[,§,#]

[†]Department of Chemistry & Biochemistry, Department of Molecular & Cellular Biosciences, College of Science and Mathematics, Rowan University, 201 Mullica Hill Road, Glassboro, New Jersey 08028, United States

[‡]Cooper Medical School of Rowan University, 401 Broadway, Camden, New Jersey 08103, United States

[§]Department of Basic Pharmaceutical Sciences, Fred Wilson School of Pharmacy, High Point University, One University Parkway, High Point, North Carolina 27268, United States

[∥]Medicinal Chemistry Section, Molecular Targets and Medications Discovery Branch, National Institute on Drug Abuse-Intramural Research Program, National Institutes of Health, 333 Cassell Drive, Baltimore, Maryland 21224, United States

[⊥]Molecular Neuropharmacology Section, National Institute of Neurological Disorders and Stroke-Intramural Research Program, National Institutes of Health, Bethesda, Maryland 20892, United States

Supporting Information

ABSTRACT: The dopamine D_4 receptor (D_4R) plays important roles in cognition, attention, and decision making. Novel D_4R-selective ligands have promise in medication development for neuropsychiatric conditions, including Alzheimer's disease and substance use disorders. To identify new D_4R-selective ligands, and to understand the molecular determinants of agonist efficacy at D_4R, we report a series of eighteen novel ligands based on the classical D_4R agonist A-412997 (**1**, 2-(4-(pyridin-2-yl)piperidin-1-yl)-*N*-(*m*-tolyl)acetamide). Compounds were profiled using radioligand binding displacement assays, *β*-arrestin recruitment assays, cyclic AMP inhibition assays, and molecular dynamics computational modeling. We identified several novel D_4R-selective ($K_i \leq 4.3$ nM and >100-fold vs other D_2-like receptors) compounds with diverse partial agonist and antagonist profiles, falling into three structural groups. These compounds highlight receptor−ligand interactions that control efficacy at D_2-like receptors and may provide insights into targeted drug discovery, leading to a better understanding of the role of D_4Rs in neuropsychiatric disorders.

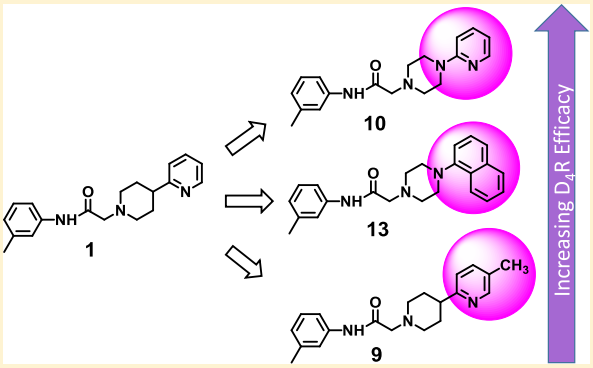

INTRODUCTION

The dopamine D_4 receptor (D_4R) is a G protein-coupled receptor and a member of the D_2-like subfamily of dopamine receptors (including D_2R, D_3R, and D_4R). D_2-like receptors have high sequence homology and share a $G_{\alpha i/o}$-coupled signaling mechanism, but differ substantially in localization within the brain and at the subcellular level.[1] Compared with D_2Rs and D_3Rs, D_4Rs have the lowest level of expression in the brain and show a unique distribution pattern, with most located in the prefrontal cortex (PFC) and hippocampus. The other D_2-like receptors are primarily in the striatum, basal ganglia, and pituitary gland regions, regions associated with D_2R-targeting antipsychotic drugs and the motor and endocrine side effects commonly observed with them.[2,3] In contrast, D_4Rs expressed in PFC and hippocampus affect attention, exploratory behavior,[3] and performance in novel object recognition[4,5] and inhibitory avoidance[6] cognitive tasks. Therefore, pharmacological activation of D_4Rs may be useful to treat cognitive deficits associated with schizophrenia[7−10] and attention-deficit/hyperactivity disorder.[10,11] Additional research has explored D_4R agonism as a strategy to reduce the adverse effects of opioid drugs like morphine.[12,13] D_4R antagonism may be useful to treat substance use disorders (SUDs), particularly psychostimulant addiction, and L-DOPA-induced dyskinesias.[10,14−20] The importance of targeting D_4Rs in treating these complex pathologies, especially with regards to the extent of receptor activation or inhibition, remains

Received: February 3, 2019
Published: March 18, 2019

DOI: 10.1021/acs.jmedchem.9b00231
J. Med. Chem. 2019, 62, 3722−3740

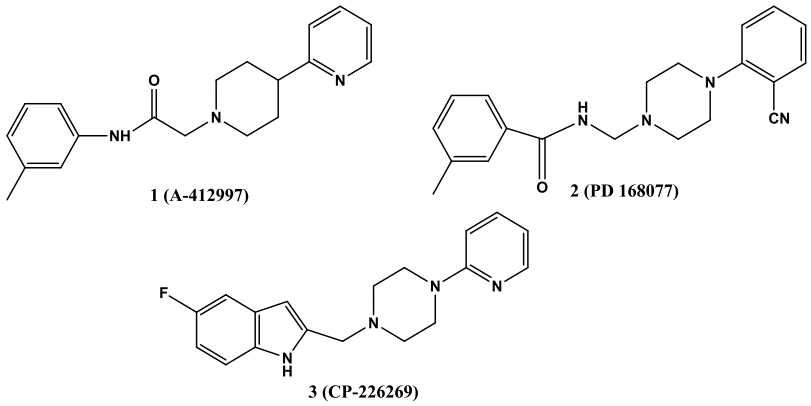

Figure 1. Three classic D_4R-selective partial agonists.

Scheme 1. Synthesis of 2-(4-(Pyridin-2-yl)piperidin-1-yl)-*N*-(*m*-tolyl)acetamide Analogues[a]

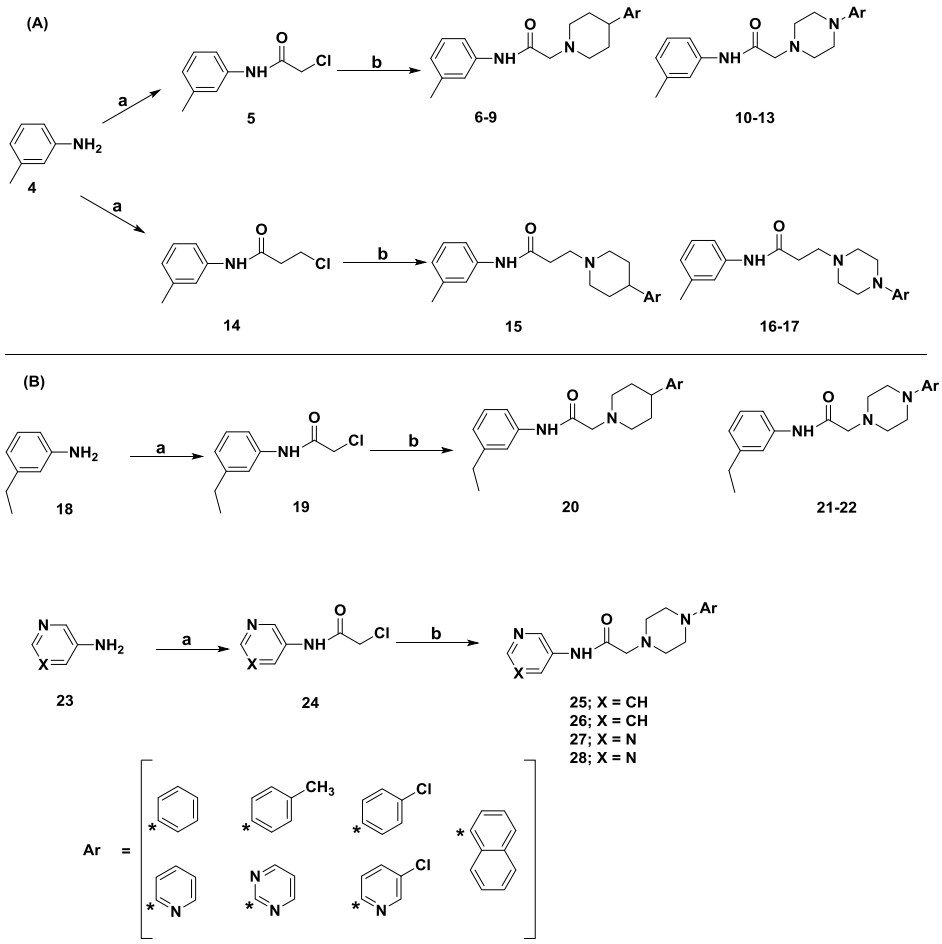

[a]Reagents and conditions: (a) triethylamine, EtOAc, RT; (b) CH_3CN, K_2CO_3, reflux, appropriate arylpiperazine or arylpiperidine.

unknown, partially because of a lack of suitable compounds for investigating these pathways.

A-412997 (**1**, 2-(4-(pyridin-2-yl)piperidin-1-yl)-*N*-(*m*-tolyl)-acetamide, Figure 1) was initially characterized as a "full agonist" (83% intrinsic activity) at D_4R, with high selectivity over D_2R and D_3R and in vivo effects that included induction of penile erection in rats.[21,22] Subsequent in vivo evaluations showed improved cognitive performance in social recognition tasks, novel object recognition tasks, and 5-trial repeated acquisition inhibitory avoidance tasks following treatment by **1** [or similar D_4R agonists PD168077 (**2**) and CP226269 (**3**)], suggesting an important role for D_4R signaling in mediating short-term memory and cognition.[5,23]

The goals of this study were to develop new D_4R agonists with a range of efficacy levels and to identify the molecular components that engender ligand efficacy at D_4R. To that end, we employed a rational drug design strategy incorporating classic structure−activity relationship (SAR) analysis around lead compound **1**. These studies were enhanced by detailed in silico molecular dynamics (MD) simulations exploiting the

DOI: 10.1021/acs.jmedchem.9b00231
J. Med. Chem. 2019, 62, 3722−3740

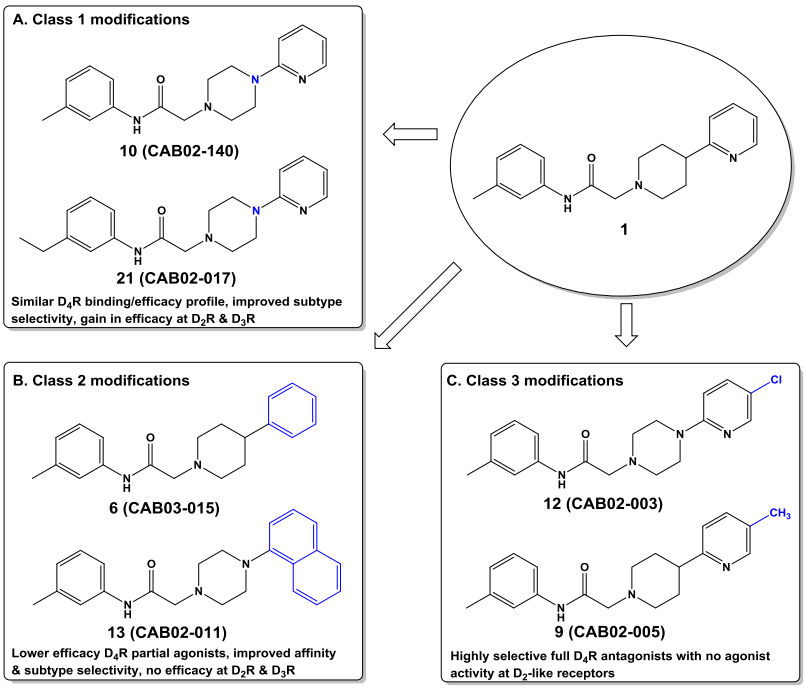

Figure 2. Three classes of modifications to the structure of **1** resulting in differing binding and efficacy profiles at D_2-like receptors. (A) Substitution of the piperidine ring for piperazine induced a gain of efficacy at D_2R and D_3R with insubstantial changes to D_4R efficacy. (B) Substitution of the pyridine ring with a phenyl or napthyl moiety produced modest D_4R subtype selectivity improvements and lowered partial agonist efficacy at D_4R with no agonist activity at D_2R or D_3R. (C) Para-substituted pyridine rings produced highly D_4R-selective antagonists.

recently reported crystal structure of D_4R.[24] Furthermore, comparative analyses were done using the D_3R crystal structure[25] and the recently reported D_2R structure.[26]

We synthesized a library of analogues primarily featuring modifications in the phenylpiperidinyl region of **1**, with additional variations in linker chain length and substitutions on the amidylphenyl region. Following extensive in vitro analyses, including binding and functional studies, we determined that selected modifications resulted in novel analogues with improved subtype selectivity. Furthermore, we identified three classes of modifications that resulted in altered efficacy profiles at all D_2-like receptors. In order to determine key receptor−ligand interactions, and identify the molecular substrates of a putative "efficacy switch," the library was docked in receptor models of D_2R, D_3R, and D_4R using MD simulations.

■ CHEMISTRY

Ligands were synthesized as outlined in Scheme 1 using routine N-alkylation reactions previously reported.[21,27] The commercially available *m*-toluidine **4** was converted to intermediate 2-chloro-*N*-(*m*-tolyl)acetamide **5** by reacting with 2-chloroacetyl chloride in the presence of triethylamine and ethyl acetate at room temperature.[28] Using the same procedure, intermediates **14**, **19**, and **24** were synthesized in a similar manner, as indicated in Scheme 1, with either a one- or two-carbon linker. The intermediate compounds **5**, **14**, **19**, and **24** were used to alkylate different commercially available arylpiperazine or arylpiperidine amines in the presence of K_2CO_3 in CH_3CN under reflux conditions to yield the desired target compounds **6**−**9**, **10**−**13**, **15**−**17**, **20**−**22**, and **25**−**28**, respectively, with the exception of the synthesis of 1-(naphthalen-1-yl)piperazine which was previously reported[29] via nucleophilic substitution reaction with naphthalen-1-amine.

■ PHARMACOLOGICAL RESULTS AND DISCUSSION

SARs at Dopamine D_2-like Receptors. A primary objective of this study was to design ligands with high D_4R binding affinity and subtype selectivity. The compound **1** and several designed analogs are shown in Figure 2. In order to obtain D_4R ligands with high affinity and selectivity, using compound **1** as our lead compound, we employed three modification strategies, creating 2-(piperidin-4-yl)pyridinyl analogs, altering the linker chain length, and creating *N*-(*m*-tolyl)acetamide analogs.

Of note, when **1** was evaluated in two different functional assays, its profile was clearly that of a partial agonist rather than a full agonist as it is often described in the literature. In the agonist mode for both the cyclic AMP (cAMP) accumulation and β-arrestin recruitment assays, **1** had an E_{max} of 61.9 and 22.5%, respectively, when normalized to dopamine.

The 2-pyridine moiety of **1** was replaced with a phenyl in **6**, *para*-tolyl in **7**, 4-chlorophenyl in **8**, and 5-methylpyridin-2-yl in **9**. The piperidine attached to the linker chain was replaced with a piperazine to form **10**, replaced with a pyrimidine to form **11**, replaced with a 5-chloropyridin-2-yl to form **12**, and replaced with a naphthyl substituent to obtain **13**. To evaluate the contribution of the alkyl chain to the binding affinity and selectivity, we synthesized alkyl chain length analogs of compounds **1**, **10**, and **11**, adding an extra methylene to the linker chain in compounds **15**, **16**, and **17**, respectively. Finally, we probed the contribution of the *N*-(3-methylphenyl)-acetamide moiety via replacement of the methyl with ethyl (compounds **20**, **21**, and **22**, compared to compounds **1**, **10**, and **12**, respectively) or replaced of the entire *N*-(3-methylphenyl)acetamide moiety with heteroaromatics (compounds **25**−**28**).

In order to best evaluate comparative affinities, two different radioligands were used in competition binding studies: [^{3}H]*N*-

DOI: 10.1021/acs.jmedchem.9b00231
J. Med. Chem. 2019, 62, 3722−3740

Table 1. Human Dopamine D_2-like Receptor Binding Data in HEK293 Membranes for Ligands with Varying Arylpiperazine and Arylamide Moieties[a]

Compound	Structure	K_i (nM) ± SEM [^{3}H]*N*-methylspiperone					K_i (nM) ± SEM [^{3}H]7-OH-DPAT				
		D_2R	D_3R	D_4R	D_2R/D_4R	D_3R/D_4R	D_2R	D_3R	D_4R	D_2R/D_4R	D_3R/D_4R
1; A-412997[21-22]	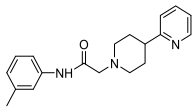	6250 ± 375	1680 ± 446	54.2 ± 7.01	115	31	251 ± 72.2	167 ± 38.8	3.95 ± 1.41	64	42
6; (CAB03-015)[22]	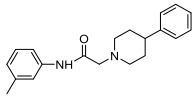	821 ± 34.9	433 ± 137	25.8 ± 9.01	32	17	127 ± 35.8	777 ± 141	1.4 ± 0.42	91	555
7; (CAB02-007HP)	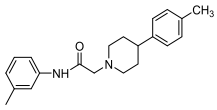	7824 ± 347	3681 ± 1237	110.4 ± 55	71	33					
8; (CAB02-009HP)	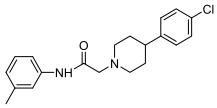	>50,000	26,320 ± 12,028	115.2 ± 42	>434	228					
9; (CAB02-005HP)	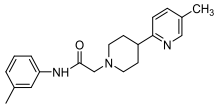	>50,000	>50,000	41.7 ± 7.0	>1198	>1198	>10,000	>10,000	6.87 ± 0.73	>1455	>1455
10; (CAB02-140)[22,27]	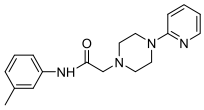	>10,000	>10,000	212 ± 62.9	>47	>47	3320 ± 450	6480 ± 972	1.89 ± 0.38	1757	3429
11; (CAB02-110)	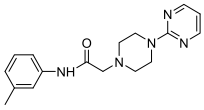	6400 ± 3800	>10,000	318 ± 95.1	20	>31	2420 ± 219	5990 ± 2040	5.66 ± 0.42	428	1058
12; (CAB02-003HP)	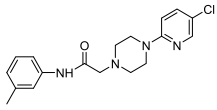	>50,000	>50,000	95 ± 26	>526	>526	>10,000	>10,000	12.5 ± 1.85	>800	>800
13; (CAB02-011HP)	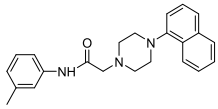	1489 ± 95	11,459 ± 3085	28.4 ± 8	52	402	200 ± 38.1	1246 ± 195	1.65 ± 0.21	121	755
15; (CAB02-120)	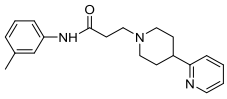	5940 ± 556	3040 ± 1350	>10,000	<0.6	<0.31	80.3 ± 28.6	510 ± 57.3	76.4 ± 7.09	1.1	6.7
16; (CAB02-142)	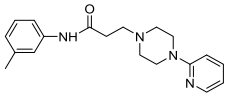	11,900 ± 2580	3790 ± 462	297 ± 34.2	40	1276	200 ± 18	781 ± 68.6	32.2 ± 8.28	6	24
17; (RNB01-007)	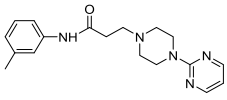	1850 ± 333	4530 ± 2010	526 ± 128	3.5	8.6	1490 ± 275	9350 ± 288	33 ± 2.52	45	2833
20; (CAB02-021HP)	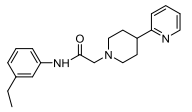	1159 ± 241	496 ± 36	82.3 ± 36	14	6.0					
21; (CAB02-017HP)	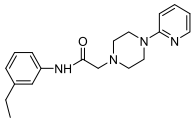	>50,000	>50,000	67.9 ± 24	>736	>736	603 ± 220	1490 ± 275	2.23 ± 0.93	270	668

DOI: 10.1021/acs.jmedchem.9b00231
J. Med. Chem. 2019, 62, 3722−3740

Table 1. continued

Compound	Structure	K_i (nM) ± SEM [^{3}H]*N*-methylspiperone					K_i (nM) ± SEM [^{3}H]7-OH-DPAT				
		D_2R	D_3R	D_4R	D_2R/D_4R	D_3R/D_4R	D_2R	D_3R	D_4R	D_2R/D_4R	D_3R/D_4R
22; (CAB02-019HP)	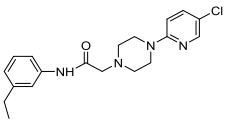	46,260 ± 3740	>50,000	172.2 ± 28	269	>290					
25; (CAB02-033HP)	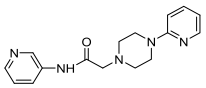	>50,000	>50,000	6407 ± 1678	>7.8	>7.8					
26; (CAB02-035HP)	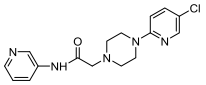	>50,000	>50,000	5000 ± 296	>10	>10					
27; (CAB02-029HP)	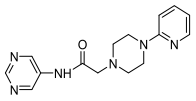	>50,000	>50,000	39,290 ± 10,710	>1.2	>1.2					
28; (CAB02-031HP)	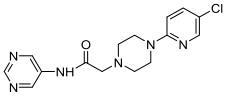	>50,000	>50,000	>50,000							

[a] K_i values determined by competitive inhibition of [^{3}H]*N*-methylspiperone or [^{3}H]-(*R*)-(+)-7-OH-DPAT binding in membranes harvested from HEK293 cells stably expressing hD_2R, hD_3R, or hD_4R. All K_i values are presented as means ± SEM.

methylspiperone, a high-affinity D_2-like antagonist, and [^{3}H]-(*R*)-(+)-7-OH-DPAT, a D_2-like agonist. Importantly, the binding affinities of D_2-like agonists and high-efficacy partial agonists are considerably higher when competing against an agonist radioligand because high-affinity agonist binding incorporates an efficacy measure in that the greater the efficacy for inducing G protein coupling, the greater the "apparent" affinity will be. On the other hand, antagonist binding, and competition for it, is unlinked from efficacy and therefore unbiased. Therefore, because these radioligands probe different receptor states, they provide complimentary views of ligand binding,[30] which are particularly valuable when examining affinity of partial agonists.

Several modifications of **1** resulted in modest improvements in D_4R affinity as measured by competition assays with [^{3}H]*N*-methylspiperone (up to ∼3-fold) and [^{3}H]-(*R*)-(+)-7-OH-DPAT (up to ∼3-fold). However, marked improvements in D_4R selectivity over D_2R and D_3R resulted from a variety of modifications, typically driven by a loss of affinity at D_2R and D_3R.

2-Pyridine substitutions resulted in a potency gain when the piperidinyl moiety was replaced with piperazinyl (e.g., **10** and **21**). Adding an extra methylene to the linker chain, as in compounds **15**, **16**, and **17**, significantly diminished D_4R affinity and selectivity. These results are consistent with previous studies that determined the importance of carboxamide linker length for D_2-like receptor selectivity.[31] Replacement of the methyl with an ethyl at the *N*-(3-methylphenyl)acetamide moiety (compounds **20**, **21**, and **22**) did not substantially alter affinity or selectivity for D_4R compared to methyl analogues **1**, **10**, and **12**, respectively. Replacement of the entire *N*-(3-methylphenyl)acetamide moiety with heteroaromatics (compounds **25**−**28**) uniformly led to loss of affinity and selectivity.

Overall, we noted three broader classes of modifications with distinct binding and efficacy profiles across the D_2-like receptors; as outlined in Figure 2, these include (1) substitution of the piperidine ring for piperazine, (2) substitution of the pyridine ring with a phenyl or napthyl moiety, and (3) para-substituted pyridine rings. These classes formed the basis for further SAR profiling and modeling studies using MD simulations.

The parent compound, **1**, showed 115-fold and 31-fold higher affinity for D_4R over D_2R and D_3R, respectively, as measured by [^{3}H]*N*-methylspiperone competition. When examined using [^{3}H]-(*R*)-(+)-7-OH-DPAT competition, **1** had higher affinity at all subtypes (consistent with an agonist radioligand being displaced by a compound that favors the activated receptor[30]) and showed a similar selectivity profile of 64-fold and 42-fold higher affinity for D_4R over D_2R and D_3R, respectively. Full binding results are presented in Table 1. Functional characterization revealed **1** to be a partial agonist at D_4R as measured in β-arrestin assays (E_{max} = 22.5%, EC_{50} = 473 nM) (Figure 3A,B) and cAMP inhibition assays (E_{max} = 61.9%, EC_{50} = 2.7 nM) (Figure 3B,C). The higher efficacy observed in the cAMP assay is likely due to spare receptors and/or amplification of cAMP accumulation versus recruitment of β-arrestin. Consistent with a partial agonist profile, **1** and related analogs were partial antagonists when run in antagonist mode (Figure 3B,D), blocking function to a similar degree as their maximal agonist activity. This would be expected for a compound that is a partial agonist that maintains affinity for the orthosteric part of the receptor, thereby acting as a partial antagonist in antagonist assays. Importantly, **1** showed no measurable agonist response on D_2R-mediated β-arrestin recruitment but behaved as a low affinity full antagonist (Figure 3E). Furthermore, **1** has very low potency and efficacy at the D_3R (Figure 3F). Complete functional results are presented in Tables 2 and 3. These data indicate that **1** is a potent and highly selective partial agonist at the D_4R.

Replacing the piperidinyl ring of **1** with a piperazine (Figure 2, class 1)—typified by **10** and **21**—resulted in similar binding and agonist efficacy profiles at D_4R, improved subtype selectivity (Tables 1 and 2), and a gain in efficacy at both D_2R and D_3R (Figure 3 and Tables 2 and 3). Replacing the pyridinyl ring of **1** with a phenyl or napthyl moiety (Figure 2, class 2)—typified by **6** and **13**—resulted in improved subtype selectivity, and importantly a diminished-efficacy partial agonist profile at D_4R. These compounds showed no

DOI: 10.1021/acs.jmedchem.9b00231
J. Med. Chem. 2019, 62, 3722−3740

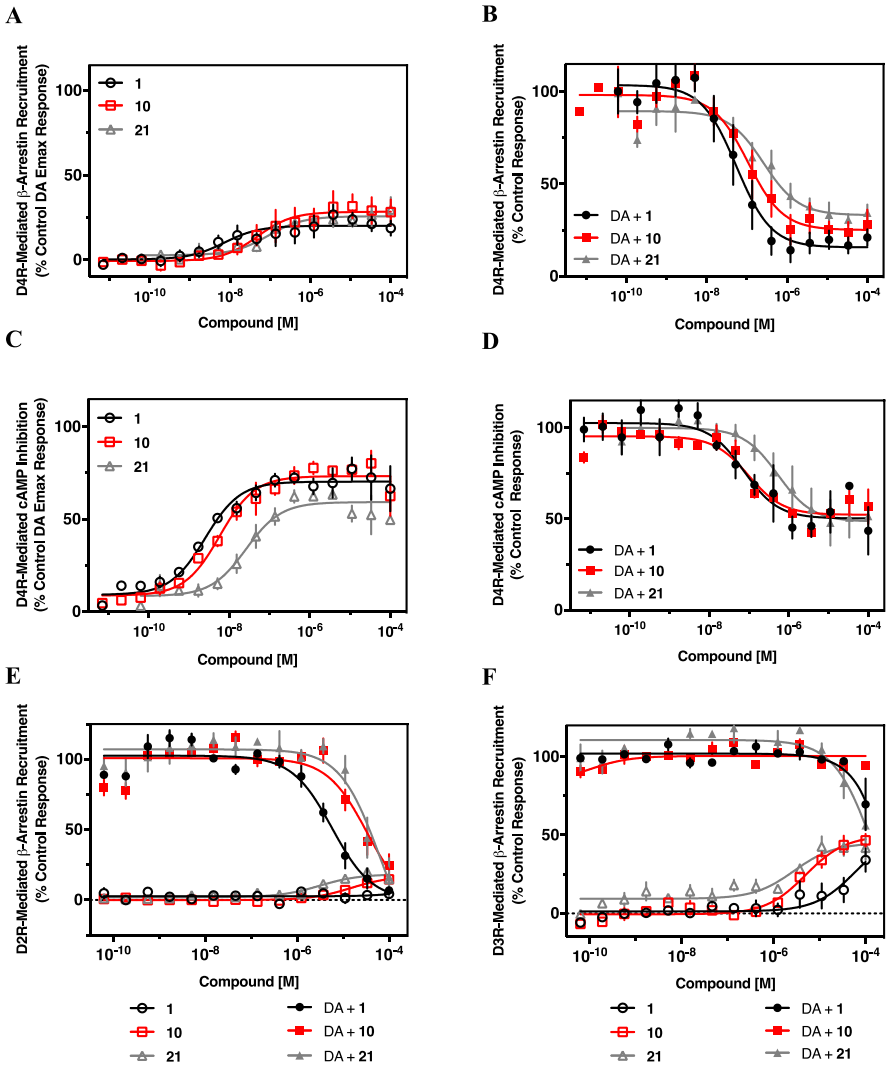

Figure 3. Compounds **10** (red) and **21** (gray) show similar pharmacology to parent compound **1** (black). D_4R-expressing stable cells lines were plated and compounds were assayed for agonist (A) and antagonist (B) activity on β-arrestin recruitment. Similarly, D_4R-mediated inhibition of cAMP accumulation was also examined in both agonist (C), and antagonist (D) modes, as indicated. Assays were conducted as described in the Experimental Methods; briefly, agonist assays were conducted by incubating the cells with the indicated concentration of test compound and measuring luminescence. Antagonist assays were conducted by incubating the compound with an EC_{80} concentration of dopamine (1 μM for β-arrestin and 10 nM in cAMP) and the indicated concentration of the test compound. For cAMP assays, cells were first stimulated with 10 μM forskolin. Agonist mode assays are expressed as a percentage of the maximum dopamine response, whereas antagonist mode assays are expressed as a percentage of dopamine's EC_{80} response. E_{max} and EC_{50} values are shown in Tables 2 and 3. Data were fit using nonlinear regression of individual experiments performed in triplicate and are shown as means ± SEM; $n = 3$. Dopamine and sulpiride were run during each assay as positive controls for a full agonist and full antagonist respectively (data not shown). Compounds were also tested for both agonist and antagonist activity on cells stably expressing the closely related D_2R (E) or D_3R (F). Assays were conducted as described in the Experimental Methods. Agonist mode assays (open symbols) are expressed as a percentage of the maximum dopamine response observed for each receptor, whereas antagonist mode assays (solid symbols) are expressed as a percentage of dopamine's EC_{80} response. E_{max} and EC_{50} values are shown in Tables 2 and 3. Data were fit using nonlinear regression of individual experiments performed in triplicate and are shown as means ± SEM; $n = 3$.

measurable agonist efficacy at either D_2R or D_3Rs (Figure 4). A para-substitution on the pyridinyl ring of **1** (Figure 2, class 3)—typified by **12** and **9**—resulted in compounds that lost all agonist efficacy but retained high-affinity binding at D_4R, with very minimal binding at D_2R or D_3R. The compounds showed potent antagonism of the D_4R response with minimal low potency D_2R blockade and no measurable affinity or efficacy at D_3R. Therefore, this class of compounds represents highly selective D_4R antagonists with no measurable agonist efficacy on any D_2-like receptor (Figure 5, Tables 1−3).

Individual compounds within classes 1−3 resulted in modest changes to overall efficacy and potency as overviewed in Tables 1−3. For this reason, we chose to focus on typified examples of a range of agonist efficacy (higher, medium, and none) at the D_4R. Using these classes, we performed MD simulations to identify interaction sites on the receptor that may play a pivotal role in engendering agonist selectivity and efficacy.

MD Studies. To gain insights on probable ligand interactions at D_4R, a set of seven ligands from the parent compound and the three class of modifications (i.e., **1**, **6**, **9**, **10**, **12**, **13**, and **21**) were docked to the crystal structures of D_2R,[26] D_3R,[25] and D_4R.[24] Each receptor−ligand combination was subjected to 100 ns MD simulations, followed by the simulation interaction diagram (SID) and clustering analysis

DOI: 10.1021/acs.jmedchem.9b00231
J. Med. Chem. 2019, 62, 3722−3740

Table 2. Efficacy as Measured via Modulation of cAMP Accumulation[a]

	D_2R efficacy				D_4R efficacy				EC_{50}	IC_{50}
compound	cAMP E_{max} %[b]	cAMP $EC_{50(nM)}$	cAMP Ant. %[c]	cAMP $IC_{50(nM)}$	cAMP E_{max} %[b]	cAMP $EC_{50(nM)}$	cAMP Ant. %[c]	cAMP $IC_{50(nM)}$	D_2R/D_4R	D_2R/D_4R
1	inactive	inactive	ND	>50000	61.9 ± 4.7	2.7 + 0.9	53.8 ± 6.0	68.4 ± 32.8	ND	>735
6	inactive	inactive	100 + 0.00	16447 + 3540	32.9 ± 3.9	15.4 ± 13.2	46.7 ± 6.0	2.0 ± 0.05	ND	8224
7	inactive	inactive	100 ± 0	44834 ± 28125	inactive	inactive	95.8 ± 2.2	3064 ± 1220	ND	15
8	inactive	inactive	97.5 ± 2.5	71437 ± 28563	inactive	inactive	100 ± 0	70157 ± 20766	ND	1.0
9	inactive	inactive	100 ± 0	71065 ± 20 585	inactive	inactive	100 ± 0	453 ± 15	ND	157
10	18.96 ± 5.2	763 ± 386	ND	>100000	64.2 ± 5.7	3.6 ± 1.3	43.2 ± 1.8	82.7 ± 37.9	214	>1210
11	54.4 ± 7.5	2092 ± 46	ND	>100000	64.6 ± 4.2	3.4 + 2.0	45.0 ± 7.7	463 ± 157	612	>216
15	83.1 ± 4.2	50.1 ± 25	ND	>100000	28.1 ± 1.6	349 ± 75	77.6 ± 5.2	6343 ± 2524	0.14	>16
16	79.7 ± 8.4	154 ± 31	ND	>100000	30.0 ± 2.1	612 ± 563	84.2 ± 6.0	1629 ± 255	0.25	>61
17	inactive	inactive	ND	>100000	13.7 ± 1.2	568 ± 456	87.0 ± 3.4	2120 ± 534	ND	>47
12	inactive	inactive	98.3 ± 1.7	66077 ± 18646	inactive	inactive	93.4 ± 2.6	4701 ± 1466	ND	14
13	inactive	inactive	100 ± 0	68329 ± 31671	27.8 ± 8.4	108.5 ± 94.3	73.8 ± 13.6	2521 ± 1067	ND	27
20	inactive	inactive	96.6 ± 3.5	16278 ± 11601	25.6 ± 7.2	539 ± 151	70.8 ± 15	1908 ± 242	ND	9
21	18.80 ± 8.19	1600 ± 396	88 ± 6.1	40466 ± 29968	58.0 ± 1.8	28.7 ± 9.9	58.4 ± 9.7	1311 ± 814	56	31
22	inactive	inactive	100 ± 0	46795 ± 27644	inactive	inactive	100 ± 0	7059 ± 1136	ND	7
25	38.6 ± 3	1965 ± 44	100 ± 0	>100000	47.3 ± 7.9	1075 ± 390	100 ± 0	86493 ± 3130	2.0	>1.1
26	inactive	inactive	100 ± 0	86617 ± 13383	inactive	inactive	100 ± 0	40000 ± 9421	ND	2
27	inactive	inactive	98.1 ± 1.5	94255 ± 5745	inactive	inactive	100 ± 0	>100000	ND	<1
28	inactive	inactive	76.2 ± 17.6	72516 ± 18052	inactive	inactive	100 ± 0	>100000	ND	<1

[a]Values determined by nonlinear regression of individual experiments run in triplicate as detailed in materials and methods under cAMP accumulation assays. All EC_{50}, IC_{50}, and E_{max} values are presented as means ± SEM; n = 3−4. ND indicates not determined due to an incomplete curve. Inactive indicates no measurable activity in indicated assay. [b]A measure of agonism as defined by the maximum inhibition of cAMP observed for each compound. [c]A measure of antagonism as defined by the maximum blockade of dopamine mediated cAMP inhibition by each compound.

as described in the Experimental Methods section. The results are included in the Supporting Information (Tables S2−S4 and Figures S2−S39). Comparisons of structural and dynamic properties of each ligand−receptor system, with reference to the parent compound **1** for each receptor system, are listed in Table S1. Although the same class modifications caused similar changes in the majority of the analyzed properties, some subtle differences are also identified. A representative ligand−receptor system from each class modification is presented here.

In order to explore class 1 modifications that showed a gain of efficacy at D_2R and D_3R with minimal changes in D_4R binding or efficacy, **10** was selected to be presented here along with parent compound **1**. The comparative ligand binding at of **10** D_2R (Figure 6) and D_3R (Figure 7) revealed that the modest ligand change—the substitution of a piperazine for a piperidine—induced a dramatic shift in the binding orientation at D_2R and D_3R: compared to the parent compound **1**, **10** took on a rotated orientation in both receptors, in which the arylamide portion of the **10** occupies a region of the binding pocket that accommodates the 2-(piperidin-4-yl)pyridinyl portion of **1**. This pose allows **10** to better engage with the conserved transmembrane (TM) 3 aspartate residue ($D^{3.32}$) located within the orthosteric binding pocket of biogenic amine receptors like dopaminergic receptors.[32] Additionally, there was new engagement with conserved $V^{2.61}$, and additional TM5 and TM6 helix shifts in both receptors. In contrast, the binding orientation of **10** at D_4R is similar to that of **1** (Figure S7), although a shift in the orientation of the pyridinylpiperidine ring system deeper into the receptor was observed. **21** docked similarly to **10** at D_2R and at D_4R (i.e., rotated 180° in comparison to **1**), but differed at D_3R in which the pose was similar to that of **1**, possibly indicating a different activation mechanism for D_3R by this compound.

13 (Figure 8), representing class 2 modifications that showed a partial loss of efficacy at D_4R, and **9** (Figure 9), representing class 3 modifications that showed a complete loss of efficacy at D_4R, are shown in models of D_4R alongside the parent compound **1**. **13** uniquely engaged with $S^{2.64}$, $E^{2.65}$, and $T^{7.39}$, and induced conformational shifts in several TM domains and intra/extracellular loops. **9** showed grater engagement with ECL2 and uniquely interacted with $C^{3.25}$ and $W^{6.48}$. Whereas **13** adopted a pose similar to **1**, **9** adopted a rotated orientation in which the arylamide portion of the **9** occupies a region of the binding pocket that accommodates the 2-(piperidin-4-yl)pyridinyl portion of **1** (Table S1). The results seen in these two comparisons are consistent with previous observations in which regiosubstitutions on an aryl ring of a terminal arylpiperazine can modulate efficacy at D_4R.[33,34] In particular, the inclusion of a para substitution on the terminal arylpiperazine has reliably produced D_4R antagonists for a wide variety of molecules with diverse substituents on the secondary pharmacophore.

DOI: 10.1021/acs.jmedchem.9b00231
J. Med. Chem. 2019, 62, 3722−3740

Table 3. Efficacy as Measured via Modulation of β-Arrestin Recruitment[a]

	D_2R efficacy				D_3R efficacy				D_4R efficacy				EC_{50}		IC_{50}	
compound	β-arr E_{max}	β-arr $EC_{50(nM)}$	β-arr Ant. %	β-arr IC_{50}	β-arr E_{max}	β-arr $EC_{50(nM)}$	β-arr Ant. %	β-arr IC_{50}	β-arr E_{max}	β-arr $EC_{50(nM)}$	β-arr Ant. %	β-arr IC_{50}	D_2R/D_4R	D_3R/D_4R	D_2R/D_4R	D_3R/D_4R
1	inactive	inactive	94.8 ± 2.8	5846 ± 1802	ND	>100000	ND	>100000	22.5 ± 3.98	473 ± 457	81.7 ± 2.7	191 ± 98	ND	>4	31	>524
6	inactive	inactive	99.7 ± 0.3	7692 ± 2301	inactive	inactive	ND	>50000	14 ± 0.3	242 ± 89	93.3 ± 1.8	135 ± 65	ND	ND	57	>371
7	inactive	inactive	100 ± 0	89153 ± 10847	inactive	inactive	inactive	inactive	inactive	inactive	100 ± 0	7352 ± 1749	ND	ND	12	ND
8	inactive	inactive	100 ± 0	>100000	inactive	inactive	inactive	inactive	inactive	inactive	100 ± 0	42357 ± 30018	ND	ND	>2	ND
9	inactive	inactive	100 ± 0	>100000	inactive	inactive	inactive	inactive	inactive	inactive	98.1 ± 2	394 ± 78	ND	ND	>254	ND
10	23.9 ± 5.1	26175 ± 12448	76.5 ± 6.9	16010 ± 5174	49.4 ± 2.0	6354 ± 2617	inactive	>100000	30.7 ± 6.4	394 ± 294	78.9 ± 3.1	313 ± 215	66	>16	51	>320
11	39.6 ± 5.3	8321 ± 3455	78.9 ± 8.6	25008 ± 5017	58.4 ± 6.6	5581 ± 1614	inactive	>100000	24.7 ± 5	278 ± 167	80.6 ± 3.0	197 ± 115	30	>20	127	>509
15	48.9 ± 6.8	2480 ± 1834	72.1 ± 7.9	7627 ± 1573	55.4 ± 1.57	970 ± 115	ND	>50000	inactive	inactive	98.7 ± 1.0	3805 ± 2944	12	>5	2.0	>26
16	44.1 ± 6.3	1455 ± 572	77.7 ± 3.7	7067 ± 2290	41.4 ± 5.83	1601 ± 867	ND	>50000	inactive	inactive	97.9 ± 1.2	1086 ± 597	ND	>1	7.0	>46
17	inactive	inactive	94.6 ± 5.4	11847 ± 2000	inactive	inactive	ND	>50000	inactive	inactive	97.1 ± 0.8	430 ± 195	ND	ND	28	>116
12	inactive	inactive	100 ± 0	>100 000	inactive	inactive	inactive	inactive	inactive	inactive	100 ± 0	7777 ± 2166	ND	ND	>13	ND
13	inactive	inactive	100 ± 0	>100 000	inactive	inactive	inactive	inactive	16.4 ± 3.9	9212 ± 6238	96.7 ± 2.7	4252 ± 1077	ND	ND	>24	ND
20	inactive	inactive	100 ± 0	67613 ± 17748	inactive	inactive	inactive	inactive	inactive	inactive	91.7 ± 6.8	2622 ± 678	ND	ND	26	ND
21	18.7 ± 0.4	3887 ± 1878	100 ± 0	88447 ± 11553	44.7 ± 5.9	2755 ± 472	100 ± 0	88 205 ± 9631	26.2 ± 5.1	133 ± 60.3	59.7 ± 4.6	370 ± 105	29	21	239	238
22	inactive	inactive	100 ± 0	70703 ± 29297	inactive	inactive	inactive	inactive	inactive	inactive	80.4 ± 6.0	10449 ± 2482	ND	ND	6.8	ND
25	21.3 ± 6.8	48503 ± 27571	inactive	inactive	18.6 ± 2.7	2802 ± 2507	inactive	inactive	19.0 ± 2.7	2657 ± 121	100 ± 0	25780 ± 9773	18	1.0	ND	ND
26	inactive	inactive	inactive	inactive	inactive	inactive	inactive	inactive	inactive	inactive	93.1 ± 7	23450 ± 11959	ND	ND	ND	ND
27	inactive	inactive	inactive	inactive	inactive	inactive	inactive	inactive	inactive	inactive	inactive	inactive	ND	ND	ND	ND
28	inactive	inactive	inactive	inactive	inactive	inactive	inactive	inactive	inactive	inactive	100 ± 0	>100000	ND	ND	ND	ND

[a]Values determined by nonlinear regression of individual experiments run in triplicate as detailed in materials and methods under β-arrestin assays. All EC_{50}, IC_{50}, and E_{max} values are presented as means ± SEM; n = 3–4. ND indicates not determined due to an incomplete curve. Inactive indicates no measurable activity in indicated assay.

DOI: 10.1021/acs.jmedchem.9b00231
J. Med. Chem. 2019, 62, 3722−3740

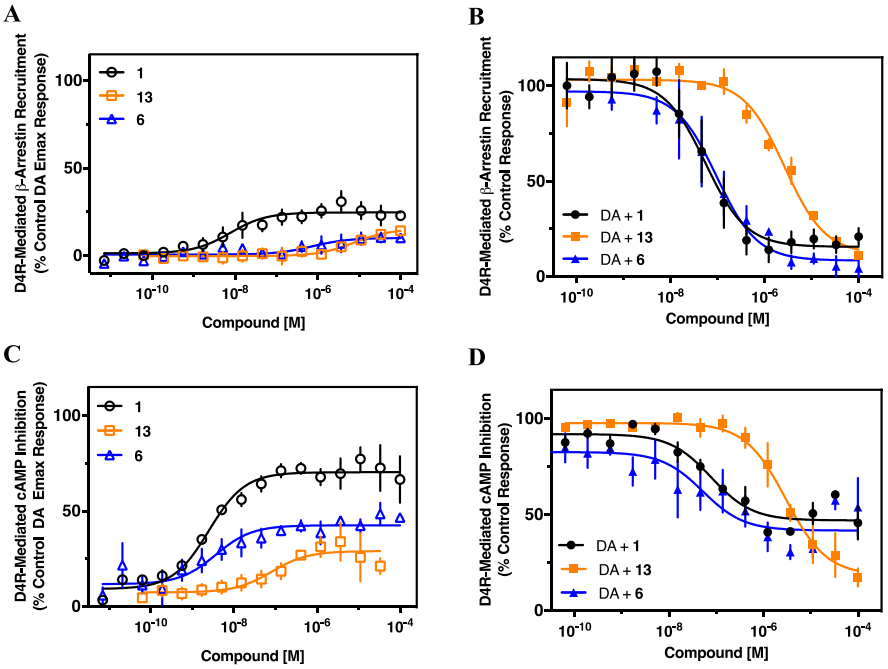

Figure 4. Compounds **13** (yellow) and **6** (blue) show diminished agonist activity at the D_4R compared to parent compound **1** (black). D_4R-expressing stable cells lines were plated and compounds were assayed for agonist (A) and antagonist (B) activity on β-arrestin recruitment. Similarly, D_4R-mediated inhibition of cAMP accumulation was also examined in both agonist (C), and antagonist (D) modes, as indicated. Assays were conducted as described in the Experimental Methods; briefly, agonist assays were conducted by incubating the cells with the indicated concentration of test compound and measuring luminescence. Antagonist assays were conducted by incubating the compound with an EC_{80} concentration of dopamine (1 μM for β-arrestin and 10 nM in cAMP) and the indicated concentration of test compound. For cAMP assays, cells were first stimulated with 10 μM forskolin. Agonist mode assays are expressed as a percentage of the maximum dopamine response, whereas antagonist mode assays are expressed as a percentage of dopamine's EC_{80} response. E_{max} and EC_{50} values are shown in Tables 2 and 3. Dopamine and sulpiride were run during each assay as positive controls for a full agonist and full antagonist, respectively (data not shown). Data were fit using nonlinear regression of individual experiments performed in triplicate and are shown as means ± SEM; $n = 3$.

■ CONCLUSIONS

Evidence from human genetic studies and animal models suggest that D_4R signaling may mediate behavioral traits including impulsivity,[35] novelty seeking,[35−38] fear and anxiety,[39,40] and sensitivity to drugs of abuse.[40−43] While modulation of postsynaptic D_4R expression in the PFC is typically hypothesized to mediate the reported in vivo effects of D_4R agonists and antagonists, evidence suggests important roles of D_4R expression in the nucleus accumbens shell[44] and within the lateral habenula,[45] in which the receptor may be preferentially activated by norepinephrine rather than dopamine.[46,47] Furthermore, little is known about the physiological relevance of independent D_4R-mediated signaling pathways (e.g., cAMP and β-arrestin) in the manifestation of behavioral outputs. A recent report identified a D_4R-selective compound containing an unsubstituted phenylpiperazine that potently and partially activated $G_{\alpha i}$ but inhibited β-arrestin2 recruitment and identified likely ligand−residue interactions that affect receptor activation states.[48] There is much left to be determined about the physiological role of D_4R signaling in modulating attention and cognitive processes, and new selective agonists and antagonists of these receptors will be valuable tools for deduction of signaling importance by these receptors.

New highly selective D_4R partial agonists and antagonists will be useful to better characterize the role of D_4R signaling in vivo. While we have primarily focused on selectivity against the very closely related D_2R and D_3R, it will be important to establish global selectivity of these compounds for in vivo experimentation through a broader screening of biogenic amine receptors. To this end, we investigated a subset of these compounds on the related D_1-like DARs. None of the tested compounds showed any measurable agonist or antagonist effect at either the D_1R or D_5R (Figure S1). Comprehensive binding and functional studies, in concert with detailed molecular modeling analyses using newly published crystal structures, provides a platform for developing high-affinity and highly subtype selective ligands of varying efficacies. This study aimed to identify key molecular interactions that dictate D_4R potency, efficacy, and subtype selectivity.

The parent compound, **1**, was confirmed to be a high-affinity (low nM K_i value) partial agonist (E_{max} = 23−62%) at D_4R. Illustrative of broader trends from our library, the compound K_i values for all D_2-like receptors determined using [^{3}H]-(*R*)-(+)-7-OH-DPAT competition assays tended to be lower (more potent) than those obtained using [^{3}H]*N*-methylspiperone. As expected, the divergence between these values increased with agonist efficacy, consistent with previous experience regarding agonist versus antagonist radioligands.[30]

Key modifications to the **1** pharmacophore provided modest gains to D_4R affinity, but dramatic gains in selectivity over D_2R and D_3R, likely because of a substantial decrease in D_2R and D_3R engagement by the analogs. Interestingly, the manner of these substitutions produced three classes of lead compound: (1) those with binding and efficacy profiles similar to **1** at D_4R but gains in efficacy at D_2R and D_3R; (2) those with improved D_4R binding and subtype selectivity with lower partial agonist efficacy; and (3) those with improved D_4R binding and

DOI: 10.1021/acs.jmedchem.9b00231
J. Med. Chem. 2019, 62, 3722−3740

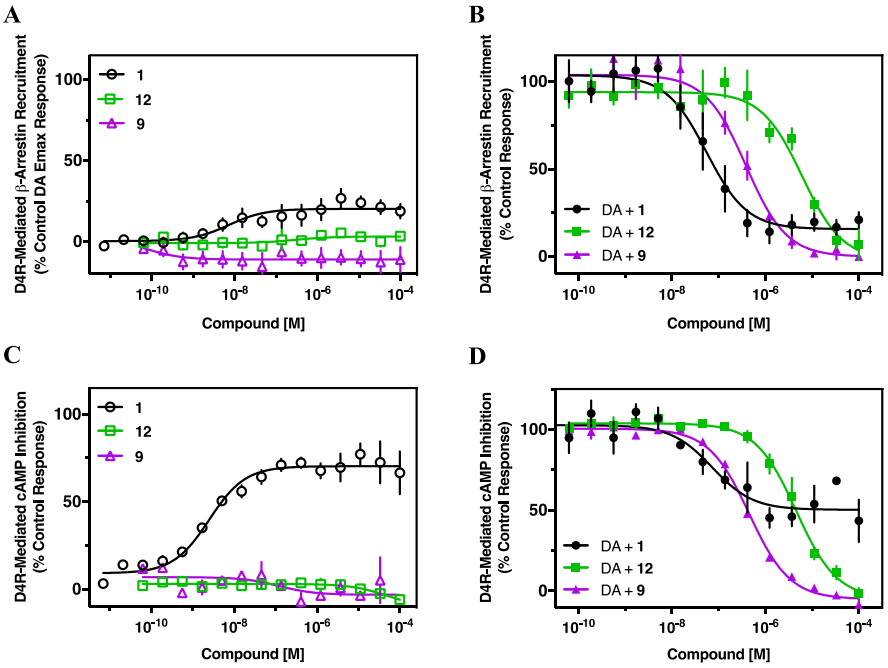

Figure 5. Compounds **12** (green) and **9** (purple) are full antagonists at the D_4R. D_4R-expressing stable cells lines were plated and compounds were assayed for agonist (A) and antagonist (B) activity on β-arrestin recruitment. Similarly, D_4R-mediated inhibition of cAMP accumulation was also examined in both agonist (C), and antagonist (D) modes, as indicated. Assays were conducted as described in the Experimental Methods; briefly, agonist assays were conducted by incubating the cells with the indicated concentration of test compound and measuring luminescence. Antagonist assays were conducted by incubating the compound with an EC_{80} concentration of dopamine (1 μM for β-arrestin and 10 nM in cAMP) and the indicated concentration of test compound. For cAMP assays, cells were first stimulated with 10 μM forskolin. Assays were conducted as described in the Experimental Methods. Agonist mode assays are expressed as a percentage of the maximum dopamine response, whereas antagonist mode assays are expressed as a percentage of dopamine's EC_{80} (1 μM in β-arrestin and 10 nM in cAMP) response. E_{max} and EC_{50} values are shown in Tables 2 and 3. Dopamine and sulpiride were run during each assay as positive controls for a full agonist and full antagonist respectively (data not shown). Data were fit using nonlinear regression of individual experiments performed in triplicate and are shown as means ± SEM; n = 3.

subtype selectivity with full antagonist characteristics. MD simulations suggest that the gain in D_2R and D_3R efficacy seen in compounds like **10** could be partially due to achieving a rotated ligand pose that more fully engages the conserved TM3 aspartate. Similarly, the complete shift to antagonism at D_4R seen in compounds like **9** could be partially due to inducing an alternate binding pose that either no longer allows full engagement of the orthosteric binding site and occupation of an alternative secondary binding pocket or a ligand-dependent alteration of the receptor energy landscape leading to the stabilization of a different receptor conformation.

These molecular models provide testable predictions relative to the unique interaction sites of these diverse compounds within the D_4R. These interactions likely underlie agonist efficacy of a given compound. Interestingly, compounds can be "rank ordered" by levels of agonist efficacy starting with **1** having the highest D_4R activation, followed by class 1 compounds (which show similar agonist efficacy) and then class 2 compounds (which show less agonist efficacy) and class 3 compounds that lack any agonist efficacy. As expected, these compounds align the opposite way for antagonist efficacy, wherein a lower agonist efficacy correlates with a higher antagonist efficacy. Examined this way, one can see that it may be possible to "dial-in" or "dial-out" levels of D_4R stimulation via adjusting compound structure, and therefore interaction sites on the receptor, leading to divergent levels of partial agonism. Future studies will involve further SAR and receptor mutagenesis studies to verify these models. We are optimistic that some of the analogues may be developed into useful in vivo research tools and plan to examine absorption, distribution, metabolism, and excretion characteristics of selected analogues. It is interesting to speculate that a collection of partial agonists with varying efficacies may allow for the fine-tuning of D_4R activation, potentially leading to a fuller understanding of functional consequences of varying signaling levels for D_4R-targeted therapeutics for neuropsychiatric disorders.

■ EXPERIMENTAL METHODS

Synthesis. Reaction conditions and yields were not optimized. Anhydrous solvents were purchased from Aldrich and were used without further purification. All other chemicals and reagents were purchased from Sigma-Aldrich Co. LLC, Combi-Blocks, TCI America, OChem Incorporation, Acros Organics, and Alfa Aesar. All amine final products were converted into either the oxalate or hydrochloride salt. Spectroscopic data and yields refer to the free base form of compounds. Flash chromatography was performed using silica gel (EMD Chemicals, Inc.; 230−400 mesh, 60 Å) by using a Teledyne ISCO CombiFlash RF system. ^{1}H NMR spectra were acquired using a Varian Mercury Plus 400 spectrometer at 400 MHz. Chemical shifts are reported in parts-per-million and referenced according to deuterated solvent for ^{1}H spectra ($CDCl_3$, 7.26, CD_3OD, 3.31 or D_2O, 4.79). Combustion analysis was performed by Atlantic Microlab, Inc., (Norcross, GA), and the results agree within ±0.4% of calculated values (Table S5). Melting point determination was conducted using a Stanford Research Systems OptiMelt automated melting point apparatus and are uncorrected. On the basis of NMR and combustion data, all final compounds are >95% pure. All compounds within this series are covered under an existing patent,[49]

DOI: 10.1021/acs.jmedchem.9b00231
J. Med. Chem. 2019, 62, 3722−3740

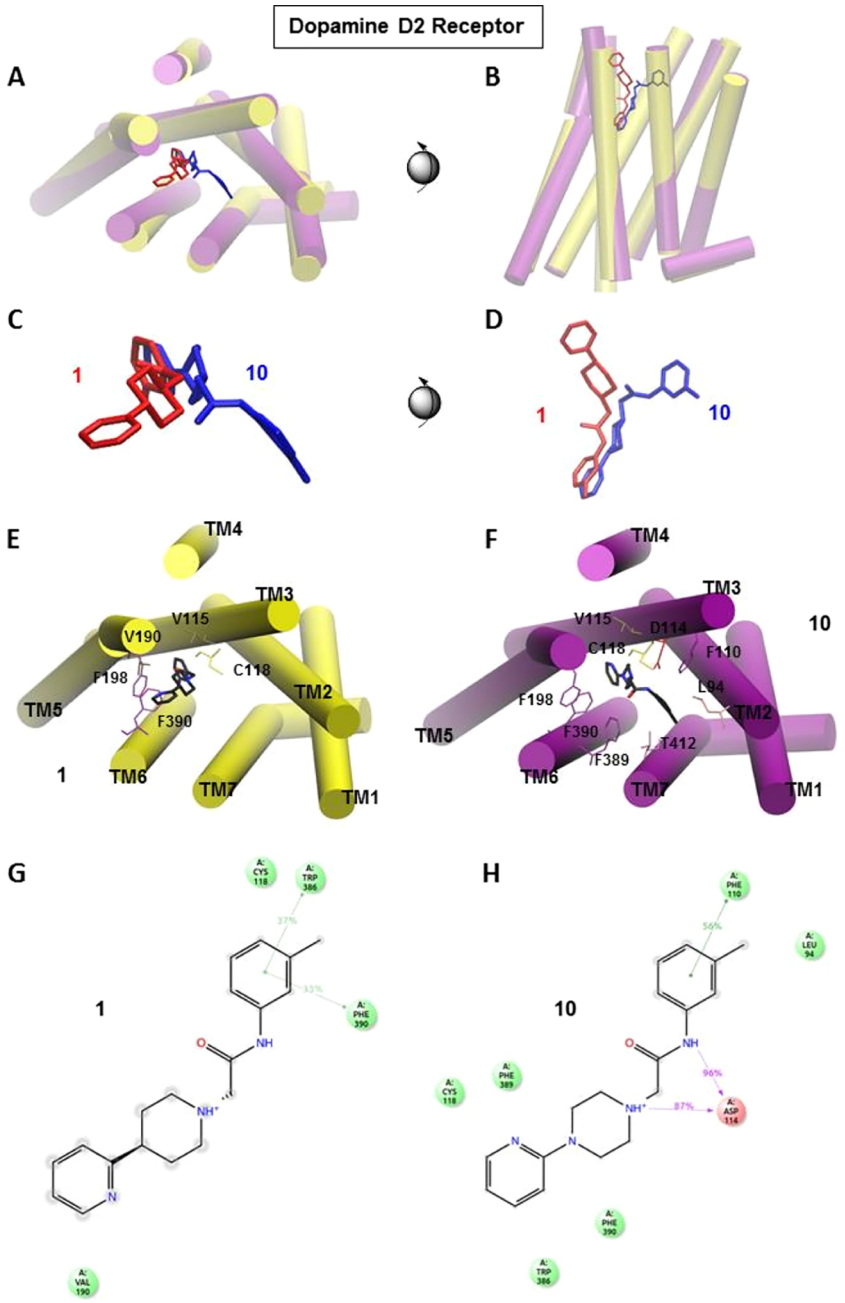

Figure 6. **1** and **10** docked at D_2R. (A−D) Comparative alignment of **1** (red ligand, yellow TM domains) and **10** (blue ligand, purple TM domains) following MD simulations of the D_2R (PDB: 6CM4[26]). (E−H) Analysis of ligand interactions with specific side chains of **1** (E,G) and **10** (F,H). Although the structural difference between **1** and **10** is only a piperidine vs a piperazine ring, this drives a dramatic shift in ligand orientation in which **10** is "flipped" and rotated by 180° about its longitudinal axis, with its pyridine ring deepest in the binding pocket. This allows the basic nitrogen of the neighboring piperazine ring to engage the conserved aspartate in TM3, a common feature of dopaminergic agonists.

but only **1**,[21,22] **6**,[22] and **10**[16,21] have been previously described in the peer-reviewed literature.

General Method A. *2-Chloro-N-(m-tolyl)acetamide (**5**).*[21,27,28] 2-Chloroacetyl chloride (1.16 g, 10.3 mmol) was added to a solution of *m*-toluidine (1.00 mL, 9.33 mmol) in ethyl acetate (30 mL) and triethylamine (1.43 mL, 10.3 mmol) at 0 °C. The reaction mixture was allowed to warm to room temperature and stirred overnight under a N_2 atmosphere. After the reaction was complete, the solvent was removed in vacuo. The crude mixture was diluted with water (100 mL) and EtOAc (100 mL) and then extracted with EtOAc (3 × 100 mL) and washed with brine (100 mL). The combined organic layer was dried over $MgSO_4$, filtered, and concentrated. The product was purified by column chromatography (10−90% EtOAc/hexanes gradient) to give **5** (1.30 g, 76% yield) as an off-white solid. ^{1}H NMR ($CDCl_3$): δ 8.19 (s, 1H), 7.38−7.33 (m, 1H), 7.26−7.22 (m, 1H), 6.99 (d, J = 7.6 Hz, 1H), 4.18 (s, 2H), 2.36 (s, 3H).

General Method B. *2-(4-Phenylpiperidin-1-yl)-N-(m-tolyl)-acetamide (**6**; CAB03-015).*[21,22,27,28] K_2CO_3 (2.57 g, 18.6 mmol) and NaI (50 mg) were added to a solution of 2-chloro-*N*-(*m*-tolyl)acetamide (570 mg, 3.10 mmol) and commercially available 4-phenylpiperidine (500 mg, 3.10 mmol) in an anhydrous acetonitrile (12 mL) solution. The reaction mixture was stirred at reflux (80 °C) for 20 h under a N_2 atmosphere. The reaction mixture was cooled to room temperature, and the solvent was removed in vacuo. The residue was diluted with water (100 mL) and EtOAc (100 mL) and then extracted with EtOAc (3 × 100 mL) and washed with brine (100 mL). The combined organic layer was dried over $MgSO_4$, filtered, and concentrated. The crude product was purified by column chromatog-

DOI: 10.1021/acs.jmedchem.9b00231
J. Med. Chem. 2019, 62, 3722−3740

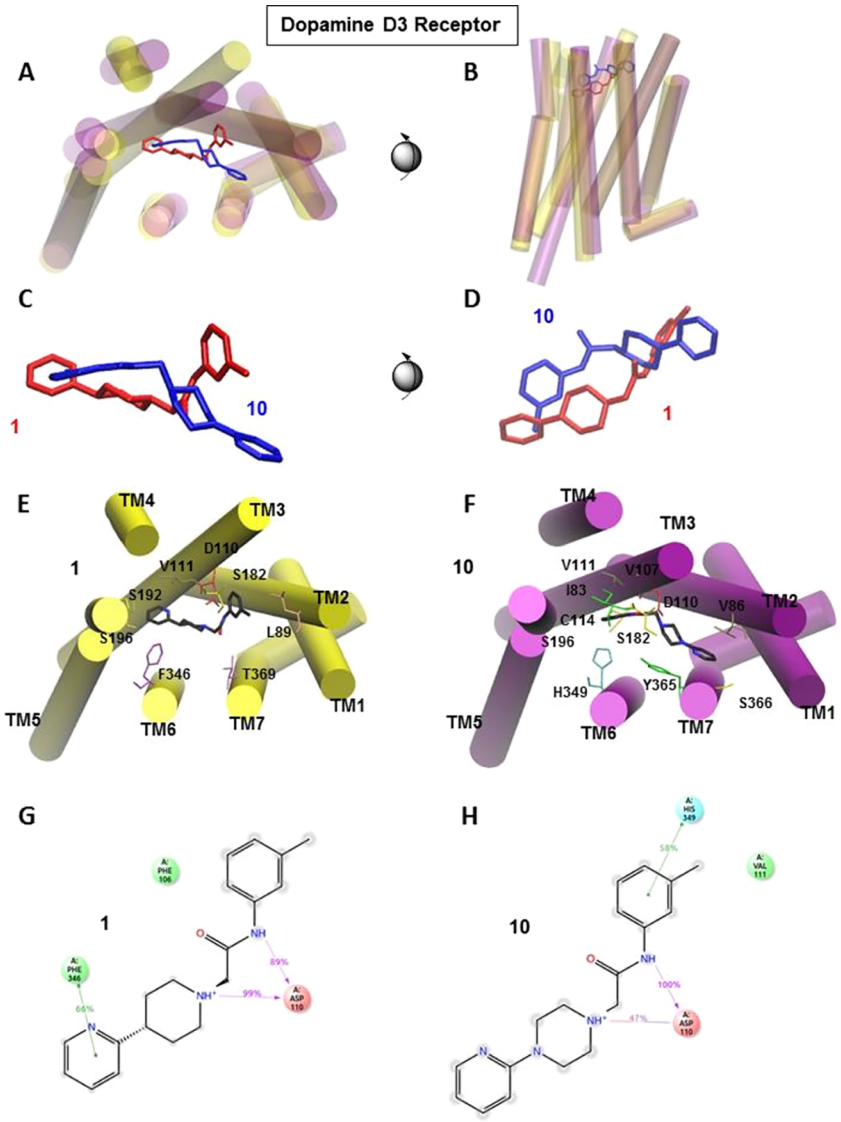

Figure 7. **1** and **10** docked at D_3R. (A−D) Comparative alignment of **1** (red ligand, yellow TM domains) and **10** (blue ligand, purple TM domains) following MD simulations of the D_3R (PDB: 3PBL[25]). (E−H) Analysis of ligand interactions with specific side chains of **1** (E,G) and **10** (F,H). As seen in the D_2R model, **10** is also "flipped" and rotated by 180° about its longitudinal axis in the binding pocket at D_3R compared to **1**. This allows for a different set of hydrophobic interactions and the engagement of the basic nitrogen of the piperazine ring to with the conserved aspartate in TM3.

raphy (10−90% EtOAc/hexanes gradient) to give pure product **6** (710 mg, 74% yield) as an off-white solid. mp 70−71 °C; ^{1}H NMR ($CDCl_3$): δ 9.15 (s, 1H), 7.42−7.40 (m, 2H), 7.38−7.31 (m, 2H), 7.24−7.20 (m, 4H), 6.93 (d, J = 7.2 Hz, 1H), 3.15 (s, 2H), 3.10−3.02 (m, 2H), 2.59−2.52 (m, 1H), 2.43−2.38 (m, 2H), 2.36 (s, 3H), 1.94−1.90 (m, 4H). Anal. ($C_{20}H_{24}N_2O{\cdot}HCl{\cdot}1/4H_2O$) C, H, N.

*N-(m-Tolyl)-2-(4-(p-tolyl)piperidin-1-yl)acetamide (**7**; CAB02-007HP).* Compound **7** was synthesized as described for **6** using K_2CO_3 (1.18 g, 8.56 mmol), NaI (40.0 mg) 4-(*p*-tolyl)piperidine (250 mg, 1.43 mmol), and 2-chloro-*N*-(*m*-tolyl)acetamide (262 mg, 1.43 mmol) in an anhydrous acetonitrile (6 mL) solution. The crude product was purified by column chromatography (15−85% EtOAc/hexanes gradient) to give pure product **7** (182 mg, 40% yield) as a white solid. mp 63−65 °C; ^{1}H NMR (400 MHz, $CDCl_3$): δ 9.23 (s, 1H), 7.47 (d, J = 15.7 Hz, 2H), 7.31 (dd, J = 14.4, 5.5 Hz, 2H), 7.23 (d, J = 2.9 Hz, 3H), 7.00 (d, J = 7.5 Hz, 1H), 3.22 (s, 2H), 3.10 (d, J = 11.4 Hz, 2H), 2.58 (d, J = 12.5 Hz, 1H), 2.49−2.46 (m, 2H), 2.43 (s, 3H), 2.41 (s, 3H), 1.91 (dt, J = 37.8, 13.1 Hz, 4H). Anal. ($C_{21}H_{26}N_2O{\cdot}1/4H_2O{\cdot}2/5C_3H_8O$) C, H, N.

*2-(4-(4-Chlorophenyl)piperidin-1-yl)-N-(m-tolyl)acetamide (**8**; CAB02-009HP).* Compound **8** was synthesized as described for **6** using K_2CO_3 (715 mg, 5.17 mmol), NaI (40.0 mg) 4-(4-chlorophenyl)piperidine (200 mg, 0.86 mmol), and 2-chloro-*N*-(*m*-tolyl)acetamide (158 mg, 0.86 mmol) in an anhydrous acetonitrile (6 mL) solution. The crude product was purified by column chromatography (40−60% EtOAc/hexanes gradient) to give pure product **8** (120 mg, 41% yield) as a light brownish solid. mp 114−116 °C; ^{1}H NMR (400 MHz, $CDCl_3$): δ 9.08 (s, 1H), 7.42−7.33 (m, 2H), 7.28 (d, J = 8.5 Hz, 1H), 7.24 (d, J = 2.4 Hz, 2H), 7.16 (d, J = 8.1 Hz, 2H), 6.95−6.88 (m, 1H), 3.13 (s, 2H), 3.01 (t, J = 7.1 Hz, 2H), 2.50 (d, J = 12.4 Hz, 1H), 2.35 (s, 2H), 2.34 (s, 3H), 1.88 (d, J = 13.1 Hz, 2H), 1.76 (q, J = 12.7 Hz, 2H). Anal. ($C_{20}H_{23}ClN_2O$) C, H, N.

*2-(4-(5-Methylpyridin-2-yl)piperidin-1-yl)-N-(m-tolyl)acetamide (**9**; CAB02-005HP).* Compound **9** was synthesized as described for **6** using K_2CO_3 (1.64 g, 11.9 mmol), NaI (40.0 mg) 5-methyl-2-(piperidin-4-yl)pyridine (350 mg, 1.98 mmol), and 2-chloro-*N*-(*m*-tolyl)acetamide (363 mg, 1.98 mmol) in an anhydrous acetonitrile (6 mL) solution. The crude product was purified by column chromatography (50−50% EtOAc/hexanes gradient) to give pure product **9** (420 mg, 66% yield) as a white solid. mp 126−128 °C; ^{1}H

DOI: 10.1021/acs.jmedchem.9b00231
J. Med. Chem. 2019, 62, 3722−3740

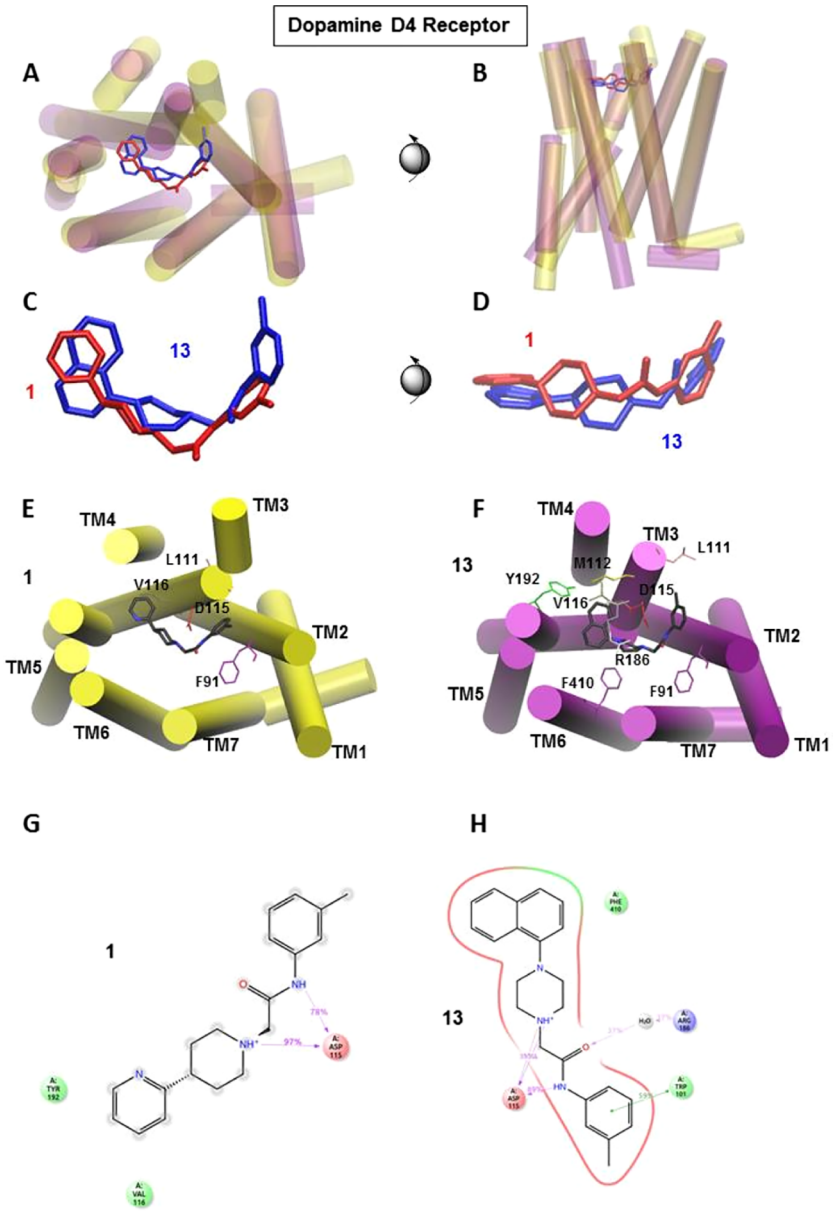

Figure 8. **1** and **13** docked at D_4R. (A–D) Comparative alignment of **1** (red ligand, yellow TM domains) and **13** (blue ligand, purple TM domains) following MD simulations of the D_4R (PDB: 5WIU[24]). (E–H) Analysis of ligand interactions with specific side chains of **1** (E,G) and **13** (F,H). The bulky napthyl ring of **13** shifts the overall fit within the extended binding pocket, partially disrupting the engagement of the basic nitrogen of the piperazine ring to with the conserved aspartate in TM3.

NMR (400 MHz, $CDCl_3$): δ 9.09 (s, 1H), 8.03 (s, 1H), 7.43–7.30 (m, 3H), 7.20 (d, J = 8.2 Hz, 1H), 6.93 (s, 1H), 6.61 (d, J = 8.5 Hz, 1H), 3.62–3.49 (m, 3H), 3.18 (br s, 2H), 2.74 (d, J = 5.8 Hz, 4H), 2.34 (s, 3H), 2.20 (s, 3H), 1.58–1.52 (m, 2H).

*2-(4-(Pyridin-2-yl)piperazin-1-yl)-N-(m-tolyl)acetamide (**10**; CAB02-140).*[22,27] Compound **10** was synthesized as described for **6** using K_2CO_3 (1.13 g, 6.78 mmol), NaI (40.0 mg) 1-(pyridin-2-yl)piperazine (222 mg, 1.36 mmol), and 2-chloro-*N*-(*m*-tolyl)-acetamide (250 mg, 1.36 mmol) in an anhydrous acetonitrile (6 mL) solution. The crude product was purified by column chromatography (20–80% EtOAc/hexanes gradient) to give pure product **10** (330 mg, 78% yield) as a white solid. mp 127–129 °C; ^{1}H NMR (400 MHz, $CDCl_3$): δ 9.09 (s, 1H), 8.21 (d, J = 4.6 Hz, 1H), 7.56–7.46 (m, 1H), 7.39 (d, J = 10.1 Hz, 2H), 7.24–7.19 (m, 1H), 6.94 (d, J = 7.4 Hz, 1H), 6.68 (q, J = 5.5, 4.4 Hz, 2H), 3.62 (t, J = 5.0 Hz, 4H), 3.19 (d, J = 3.2 Hz, 2H), 2.74 (d, J = 5.4 Hz, 4H), 2.35 (d, J = 3.2 Hz, 3H), 2.17 (br s, 4H). Anal. ($C_{18}H_{22}N_4O{\cdot}2HCl{\cdot}H_2O$) C, H, N.

*2-(4-(Pyrimidin-2-yl)piperazin-1-yl)-N-(m-tolyl)acetamide (**11**; CAB02-110).* Compound **11** was synthesized as described for **6** using K_2CO_3 (1.13 g, 1.16 mmol), 2-(piperazin-1-yl)pyrimidine (223 mg, 1.36 mmol), and 2-chloro-*N*-(*m*-tolyl)acetamide (250 mg, 1.36 mmol) in an anhydrous acetonitrile (6 mL) solution. The crude product was purified by column chromatography (10–90% EtOAc/hexanes gradient) to give pure product **11** (310 mg, 73% yield) as a cream solid. mp 92–94 °C; ^{1}H NMR (400 MHz, $CDCl_3$): δ 9.16–9.01 (m, 1H), 8.37–8.27 (m, 2H), 7.39 (d, J = 14.2 Hz, 2H), 7.22 (d, J = 8.1 Hz, 1H), 6.94 (d, J = 8.4 Hz, 1H), 6.53 (d, J = 4.6 Hz, 1H), 3.91 (s, 4H), 3.18 (q, J = 2.1, 1.6 Hz, 2H), 2.69 (d, J = 5.6 Hz, 4H), 2.36 (s, 3H). Anal. ($C_{17}H_{21}N_5O{\cdot}2HCl{\cdot}1.75H_2O$) C, H, N.

*2-(4-(5-Chloropyridin-2-yl)piperazin-1-yl)-N-(m-tolyl)acetamide (**12**; CAB02-003HP).* Compound **12** was synthesized as described for **6** using K_2CO_3 (1.78 g, 12.86 mmol), NaI (40.0 mg), 1-(5-chloropyridin-2-yl)piperazine (422 mg, 2.14 mmol), and 2-chloro-*N*-(*m*-tolyl)acetamide (400 mg, 2.14 mmol) in an anhydrous acetonitrile (6 mL) solution. The crude product was purified by column

DOI: 10.1021/acs.jmedchem.9b00231
J. Med. Chem. 2019, 62, 3722–3740

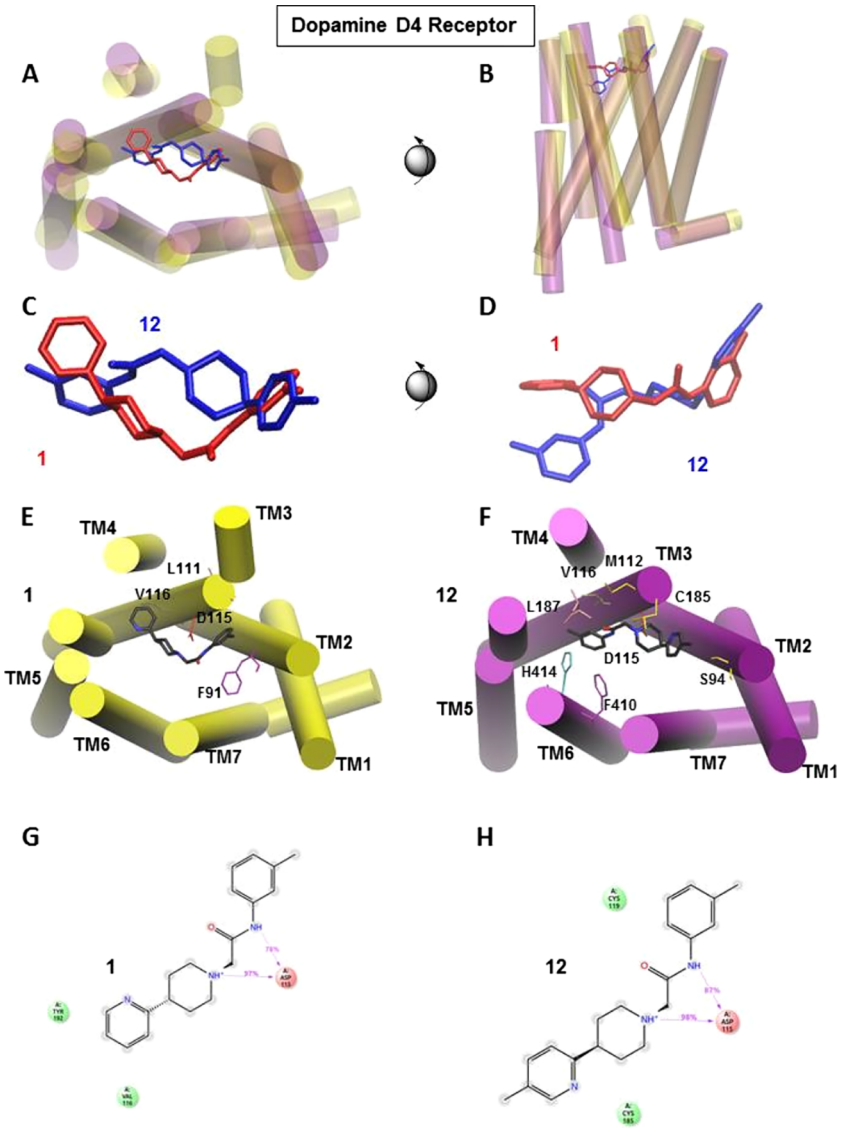

Figure 9. **1** and **9** docked at D_4R. (A−D) Comparative alignment of **1** (red ligand, yellow TM domains) and **9** (blue ligand, purple TM domains) following MD simulations of the D_4R (PDB: 5WIU[24]). (E−H) Analysis of ligand interactions with specific side chains of **1** (E,G) and **9** (F,H). The inclusion of a single para substitution on the pyridine ring of **9** induces a "flipped" orientation of the ligand, in which the binding pose is rotated by 180° about its longitudinal axis, with its pyridine ring deepest in the binding pocket driving the arylamide into a deeper binding position.

chromatography (20−80% EtOAc/hexanes gradient) to give pure product **12** (490 mg, 65% yield) as a white solid. mp 107−109 °C; ^{1}H NMR (400 MHz, $CDCl_3$): δ 9.02 (s, 1H), 8.11 (d, J = 3.3 Hz, 1H), 7.47−7.40 (m, 1H), 7.36 (d, J = 11.8 Hz, 2H), 7.19 (d, J = 8.5 Hz, 1H), 6.95−6.88 (m, 1H), 6.59 (d, J = 8.9 Hz, 1H), 3.58 (t, J = 5.2 Hz, 4H), 3.17 (d, J = 2.8 Hz, 2H), 2.71 (t, J = 5.0 Hz, 4H), 2.33 (s, 3H). Anal. ($C_{18}H_{21}ClN_4O{\cdot}2HCl{\cdot}1/2H_2O$) C, H, N.

*2-(4-(Naphthalen-1-yl)piperazin-1-yl)-N-(m-tolyl)acetamide (**13**; CAB02-011HP).* Compound **13** was synthesized as described for **6** using K_2CO_3 (2.62 g, 18.9 mmol), NaI (50.0 mg), 1-(naphthalen-1-yl)piperazine[29] (670 mg, 3.16 mmol), and 2-chloro-*N*-(*m*-tolyl)-acetamide (580 mg, 3.16 mmol) in an anhydrous acetonitrile (6 mL) solution. The crude product was purified by column chromatography (40−60% EtOAc/hexanes gradient) to give pure product **13** (546 mg, 48% yield) as a brown oil; ^{1}H NMR (400 MHz, $CDCl_3$): δ 9.17 (s, 1H), 8.20 (d, J = 7.5 Hz, 1H), 7.85 (s, 1H), 7.60 (d, J = 8.2 Hz, 1H), 7.55−7.47 (m, 2H), 7.43 (d, J = 11.4 Hz, 3H), 7.24 (d, J = 8.4 Hz, 1H), 7.15 (d, J = 7.3 Hz, 1H), 6.96 (d, J = 7.4 Hz, 1H), 3.34−3.27 (m, 2H), 3.23 (br s, 4H), 2.95 (br s, 4H), 2.38 (s, 3H). Anal. ($C_{23}H_{25}N_3O{\cdot}2HCl$) C, H, N.

*3-Chloro-N-(m-tolyl)propanamide (**14**).* Compound **14** was synthesized as described for **5** by adding 3-chloropropanoyl chloride (1.30 g, 10.3 mmol) to a solution of *m*-toluidine (1 mL, 9.33 mmol) in ethyl acetate (30 mL) and triethylamine (1.44 mL). The crude product was purified by column chromatography (20−80% EtOAc/hexanes gradient) to give compound **14** (1.43 g, 78% yield) as a white solid. ^{1}H NMR ($CDCl_3$): δ 7.44 (s, 1H), 7.36−7.22 (m, 2H), 6.99 (d, J = 7.4 Hz, 1H), 3.96−3.92 (m, 2H), 2.85 (t, J = 6.3 Hz, 2H), 2.39 (s, 3H).

*3-(4-(Pyridin-2-yl)piperidin-1-yl)-N-(m-tolyl)propanamide (**15**; CAB02-120).* Compound **15** was synthesized as described for **6** using K_2CO_3 (1.26 g, 7.56 mmol), NaI (50.0 mg), 2-(piperidin-4-yl)pyridine (246 mg, 1.52 mmol), and 3-chloro-*N*-(*m*-tolyl)-propanamide (300 mg, 1.52 mmol) in an anhydrous acetonitrile (6 mL) solution. The crude product was purified by column chromatography (50−50% EtOAc/hexanes gradient) to give pure product **15** (325 mg, 66% yield) as a light brown oil; ^{1}H NMR (400 MHz, $CDCl_3$): δ 11.08 (s, 1H), 8.55 (d, J = 4.6 Hz, 1H), 7.69−7.61 (m, 1H), 7.45 (s, 1H), 7.29 (d, J = 7.5 Hz, 1H), 7.23−7.12 (m, 3H), 6.88 (d, J = 7.5 Hz, 1H), 3.21 (d, J = 11.2 Hz, 2H), 2.87−2.70 (m, 3H), 2.53 (t, J = 5.7 Hz, 2H), 2.34 (s, 3H), 2.24 (t, J = 11.6 Hz, 2H),

DOI: 10.1021/acs.jmedchem.9b00231
J. Med. Chem. 2019, 62, 3722−3740

2.09 (d, J = 13.2 Hz, 2H), 2.02−1.87 (m, 2H). Anal. ($C_{20}H_{25}N_3O$·2HCl·3.5H_2O) C, H, N.

*3-(4-(Pyridin-2-yl)piperazin-1-yl)-N-(m-tolyl)propanamide (**16**; CAB02-142).* Compound **16** was synthesized as described for **6** using K_2CO_3 (1.26 g, 9.12 mmol), 1-(pyridin-2-yl)piperazine (248 mg, 1.52 mmol), and 3-chloro-*N*-(*m*-tolyl)propanamide (300 mg, 1.52 mmol) in an anhydrous acetonitrile (6 mL) solution. The crude product was purified by column chromatography (50−50% EtOAc/hexanes gradient) to give pure product **16** (350 mg, 71% yield) as a white solid. mp 99−101 °C; ^{1}H NMR (400 MHz $CDCl_3$): δ 10.74 (s, 1H), 8.21 (br s, 1H), 7.51 (d, J = 8.0 Hz, 1H), 7.40 (s, 1H), 7.24 (d, J = 5.7 Hz, 1H), 7.15 (td, J = 8.2, 3.3 Hz, 1H), 6.86 (d, J = 7.3 Hz, 1H), 6.68 (q, J = 7.4, 5.6 Hz, 2H), 3.64 (d, J = 6.4 Hz, 4H), 2.81−2.65 (m, 6H), 2.55 (q, J = 4.7 Hz, 2H), 2.30 (s, 3H). Anal. ($C_{19}H_{24}N_4O$·3HCl) C, H, N.

*3-(4-(Pyrimidin-2-yl)piperazin-1-yl)-N-(m-tolyl)propanamide (**17**; RNB01-007).* Compound **17** was synthesized as described for **6** using K_2CO_3 (1.26 g, 9.12 mmol), 2-(piperazin-1-yl)pyrimidine (249 mg, 1.52 mmol), and 3-chloro-*N*-(*m*-tolyl)propanamide (350 mg, 1.52 mmol) in an anhydrous acetonitrile (6 mL) solution. The crude product was purified by column chromatography (50−50% EtOAc/hexanes gradient) to give pure product **17** (321 mg, 56% yield) as a cream solid. mp 85−86 °C; ^{1}H NMR (400 MHz, $CDCl_3$): δ 10.76 (s, 1H), 8.33 (dt, J = 5.1, 2.4 Hz, 2H), 7.40 (s, 1H), 7.32−7.23 (m, 1H), 7.21−7.13 (m, 1H), 6.88 (d, J = 7.5 Hz, 1H), 6.54 (dp, J = 5.0, 2.6, 2.1 Hz, 1H), 3.94 (t, J = 4.8 Hz, 4H), 2.77 (t, J = 5.7 Hz, 2H), 2.67 (t, J = 4.6 Hz, 4H), 2.57 (q, J = 5.7, 5.0 Hz, 2H), 2.32 (s, 3H). Anal. ($C_{18}H_{23}N_5O$·HCl) C, H, N.

*2-Chloro-N-(3-ethylphenyl)acetamide (**19**).* Compound **19** was synthesized as described for **5** by adding 2-chloroacetyl chloride (3.62 mL, 45.4 mmol) to a solution of 3-ethylaniline (5.13 mL, 41.3 mmol) in ethyl acetate (30 mL) and triethylamine (1.44 mL). The crude product was purified by column chromatography (20−80% EtOAc/hexanes gradient) to give compound **19** (8.00 g, 98% yield) as a cream solid. ^{1}H NMR (400 MHz, $CDCl_3$): δ 8.23 (s, 1H), 7.47−7.38 (m, 2H), 7.32−7.27 (m, 1H), 7.04 (d, J = 7.5 Hz, 1H), 4.20 (s, 2H), 2.75−2.58 (m, 2H), 1.28−1.22 (m, 3H).

*N-(3-Ethylphenyl)-2-(4-(pyridin-2-yl)piperidin-1-yl)acetamide (**20**; CAB02-021HP).* Compound **20** was synthesized as described for **6** using K_2CO_3 (1.54 g, 11.17 mmol), 2-(piperidin-4-yl)pyridine (300 mg, 1.86 mmol), and 2-chloro-*N*-(3-ethylphenyl)acetamide (368 mg, 1.86 mmol) in an anhydrous acetonitrile (6 mL) solution. The crude product was purified by column chromatography (40−60% EtOAc/hexanes gradient) to give pure product **20** (435 mg, 73% yield) as a white solid. mp 56−58 °C; ^{1}H NMR (400 MHz, $CDCl_3$): δ 9.16 (s, 1H), 7.48−7.38 (m, 2H), 7.33 (d, J = 7.4 Hz, 2H), 7.26 (br s, 4H), 6.97 (d, J = 7.5 Hz, 1H), 3.16 (d, J = 3.3 Hz, 2H), 3.05 (d, J = 11.5 Hz, 2H), 2.66 (d, J = 7.9 Hz, 2H), 2.60−2.54 (m, 1H), 2.40 (t, J = 12.0 Hz, 2H), 1.87 (dt, J = 38.0, 13.2 Hz, 4H), 1.25 (t, J = 7.3, 5.9 Hz, 3H). Anal. ($C_{20}H_{25}N_3O$·$C_2H_2O_4$) C, H, N.

*N-(3-Ethylphenyl)-2-(4-(pyridin-2-yl)piperazin-1-yl)acetamide (**21**; CAB02-017HP).* Compound **21** was synthesized as described for **6** using K_2CO_3 (2.74 g, 19.8 mmol), 1-(pyridin-2-yl)piperazine (539 mg, 3.30 mmol), and 2-chloro-*N*-(3-ethylphenyl)acetamide (650 mg, 3.30 mmol) in an anhydrous acetonitrile (8 mL) solution. The crude product was purified by column chromatography (50−50% EtOAc/hexanes gradient) to give pure product **21** (792 mg, 74% yield) as a white solid. mp 109−111 °C; ^{1}H NMR (400 MHz, $CDCl_3$): δ 9.07 (s, 1H), 8.19 (s, 1H), 7.54−7.44 (m, 1H), 7.38 (d, J = 8.0 Hz, 2H), 7.27−7.20 (m, 1H), 6.95 (d, J = 7.6 Hz, 1H), 6.66 (d, J = 8.6 Hz, 2H), 3.60 (d, J = 6.0 Hz, 4H), 3.17 (t, J = 2.3 Hz, 2H), 2.73 (d, J = 5.0 Hz, 4H), 2.61 (t, J = 8.0 Hz, 2H), 1.26−1.15 (m, 3H). Anal. ($C_{19}H_{24}N_4O$·2HCl·3/4H_2O) C, H, N.

*2-(4-(5-Chloropyridin-2-yl)piperazin-1-yl)-N-(3-ethylphenyl)-acetamide (**22**; CAB02-019HP).* Compound **22** was synthesized as described for **6** using K_2CO_3 (1.26 g, 9.12 mmol), 1-(5-chloropyridin-2-yl)piperazine (300 mg, 1.52 mmol), and 2-chloro-*N*-(3-ethylphenyl)acetamide (300 mg, 1.52 mmol) in an anhydrous acetonitrile (6 mL) solution. The crude product was purified by column chromatography (20−80% EtOAc/hexanes gradient) to give pure product **22** (480 mg, 88% yield) as a white solid. mp 101−103 °C; ^{1}H NMR (400 MHz, $CDCl_3$): δ 9.03 (s, 1H), 8.11 (s, 1H), 7.46−7.34 (m, 3H), 7.25−7.23 (m, 1H), 6.95 (d, J = 7.5 Hz, 1H), 6.59 (d, J = 8.9 Hz, 1H), 3.57 (t, J = 4.9 Hz, 4H), 3.17 (d, J = 2.7 Hz, 2H), 2.71 (t, J = 4.7 Hz, 4H), 2.61 (t, J = 8.1 Hz, 2H), 1.32−1.13 (m, 3H). Anal. ($C_{19}H_{23}ClN_4O$·2HCl·3/4H_2O) C, H, N.

*2-Chloro-N-(pyridin-3-yl)acetamide (**24a**).* Compound **24a** was synthesized as described for **5** by adding 2-chloroacetyl chloride (0.71 mL, 17.5 mmol) to a solution of pyridin-3-amine (1.50 g, 16.0 mmol) in ethyl acetate (25 mL) and triethylamine (0.4 mL). The crude product was purified by column chromatography (20−80% EtOAc/hexanes gradient) to give **24a** (1.17 g, 43% yield) as a white solid. ^{1}H NMR (400 MHz, D_2O): δ 9.37−9.08 (m, 1H), 8.60−8.32 (m, 2H), 8.06−7.87 (m, 1H), 5.67 (s, 2H).

*2-Chloro-N-(pyrimidin-5-yl)acetamide (**24b**).* Compound **24b** was synthesized as described for **5** by adding 2-chloroacetyl chloride (0.46 mL, 5.78 mmol) to a solution of pyrimidin-5-amine (500 mg, 5.26 mmol) in ethyl acetate (10 mL) and triethylamine (0.4 mL). The crude product was purified by column chromatography (20−80% EtOAc/hexanes gradient) to give **24b** (510 mg, 57% yield) as a brown solid. ^{1}H NMR (400 MHz, D_2O): δ 9.17 (s, 1H), 8.54 (s, 2H), 8.01 (s, 1H), 5.66 (s, 2H).

*2-(4-(Pyridin-2-yl)piperazin-1-yl)-N-(pyridin-3-yl)acetamide (**25**; CAB02-033HP).* Compound **25** was synthesized as described for **6** using K_2CO_3 (1.27 g, 9.17 mmol), 1-(pyridin-2-yl)piperazine (249 mg, 1.52 mmol), and compound **24a** 2-chloro-*N*-(pyridin-3-yl)-acetamide (260 mg, 1.52 mmol) in an anhydrous acetonitrile (6 mL) solution. The crude product was purified by column chromatography (20−80% EtOAc/hexanes gradient) to give pure product **25** (287 mg, 63% yield) as a white solid. mp 173−174 °C; ^{1}H NMR (400 MHz $CDCl_3$): δ 9.23 (s, 1H), 8.59 (s, 1H), 8.37 (s, 1H), 8.23 (d, J = 12.8 Hz, 2H), 7.51 (s, 1H), 6.68 (d, J = 8.1 Hz, 2H), 3.63 (br s, 4H), 3.23 (d, J = 2.9 Hz, 2H), 2.76 (br s, 4H). Anal. ($C_{16}H_{19}N_5O$·4HCl·1.1H_2O·1/4C_3H_8O) C, H, N.

*2-(4-(5-Chloropyridin-2-yl)piperazin-1-yl)-N-(pyridin-3-yl)-acetamide (**26**; CAB02-035HP).* Compound **26** was synthesized as described for **6** using K_2CO_3 (2.63 g, 19.0 mmol), 1-(5-chloropyridin-2-yl)piperazine (627 mg, 3.17 mmol), and compound **24a** 2-chloro-*N*-(pyridin-3-yl)acetamide (540 mg, 3.17 mmol) in an anhydrous acetonitrile (6 mL) solution. The crude product was purified by column chromatography (20−80% EtOAc/hexanes gradient) to give pure product **26** (721 mg, 68% yield) as a white solid. mp 155−156 °C; ^{1}H NMR (400 MHz, $CDCl_3$): δ 9.17 (s, 1H), 8.57 (s, 1H), 8.36 (br s, 1H), 8.22 (d, J = 8.2 Hz, 1H), 8.12 (s, 1H), 7.49−7.39 (m, 1H), 7.31−7.27 (m, 1H), 6.60 (d, J = 9.1 Hz, 1H), 3.59 (s, 4H), 3.25−3.15 (m, 2H), 2.74 (d, J = 5.0 Hz, 4H). Anal. ($C_{16}H_{18}ClN_5O$·4HCl·H_2O·1/2C_3H_8O) C, H, N.

*2-(4-(Pyridin-2-yl)piperazin-1-yl)-N-(pyrimidin-5-yl)acetamide (**27**; CAB02-029HP).* Compound **27** was synthesized as described for **6** using K_2CO_3 (1.45 g, 10.5 mmol), 1-(pyridin-2-yl)piperazine (285 mg, 1.75 mmol), and compound **24b** 2-chloro-*N*-(pyrimidin-5-yl)acetamide (300 mg, 1.75 mmol) in an anhydrous acetonitrile (6 mL) solution. The crude product was purified by column chromatography (20−80% EtOAc/hexanes gradient) to give pure product **27** (268 mg, 51% yield) as a white solid. mp 144−146 °C; ^{1}H NMR (400 MHz, $CDCl_3$): δ 9.17 (s, 1H), 9.02−8.81 (m, 3H), 8.13 (br s, 1H), 7.43 (br s, 1H), 6.60 (br s, 2H), 3.56 (br s, 4H), 3.18 (br s, 2H), 2.69 (br s, 4H). Anal. ($C_{15}H_{18}N_6O$·3/2$C_2H_2O_4$·3/4H_2O) C, H, N.

*2-(4-(5-Chloropyridin-2-yl)piperazin-1-yl)-N-(pyrimidin-5-yl)-acetamide (**28**; CAB02-031HP).* Compound **28** was synthesized as described for **6** using K_2CO_3 (866 mg, 6.26 mmol), 1-(5-chloropyridin-2-yl)piperazine (207 mg, 1.04 mmol), and compound **24b** 2-chloro-*N*-(pyrimidin-5-yl)acetamide (180 mg, 1.04 mmol) in an anhydrous acetonitrile (6 mL) solution. The crude product was purified by column chromatography (20−80% EtOAc/hexanes gradient) to give pure product **28** (157 mg, 45% yield) as a yellowish oil; ^{1}H NMR (400 MHz, $CDCl_3$): δ 9.21 (s, 1H), 9.08−8.98 (m, 3H), 8.15 (d, J = 3.7 Hz, 1H), 7.47 (d, J = 8.9 Hz, 1H), 6.63 (d, J = 9.2 Hz,

DOI: 10.1021/acs.jmedchem.9b00231
J. Med. Chem. 2019, 62, 3722−3740

1H), 3.62 (br s, 4H), 3.30−3.23 (m, 2H), 2.77 (br s, 4H). Anal. ($C_{15}H_{17}ClN_6O{\cdot}C_2H_2O_4{\cdot}1.5H_2O$) C, H, N.

Radioligand Binding Studies. HEK293 cells stably expressing human $D_{2L}R$, D_3R, or $D_{4.4}R$ were grown in a 50:50 mix of Ham's F12 and Dulbecco's modified Eagle's medium culture media, supplemented with 2 mM L-glutamine, 20 mM *N*-(2-hydroxyethyl)-piperazine-*N*′-ethanesulfonic acid (HEPES), 0.1 mM non-essential amino acids, 1× antibiotic/antimycotic, 10% heat-inactivated fetal bovine serum, and 200 μg/mL hygromycin (Life Technologies, Grand Island, NY) and grown in an incubator at 37 °C and 5% CO_2. Upon reaching 80−90% confluence, cells were harvested using pre-mixed Earle's balanced salt solution (EBSS) with 5 mM ethylenediaminetetraacetic acid (EDTA) (Life Technologies) and centrifuged at 3000 rpm for 10 min at 21 °C. The supernatant was removed and the cell pellet was resuspended in 10 mL hypotonic lysis buffer (5 mM Tris, 5 mM $MgCl_2$, pH 7.4 at 4 °C) and then centrifuged at 20000 rpm for 30 min at 4 °C. The membrane pellet was resuspended in fresh binding buffer for either [^{3}H]*N*-methylspiperone (PerkinElmer, Waltham, MA) binding experiments [fresh EBSS buffer made from 8.7 g/L Earle's balanced salts without phenol red (US Biological, Salem, MA), 2.2 g/L sodium bicarbonate, pH 7.4] or [^{3}H]-(*R*)-(+)-7-OH-DPAT (ARC, Saint Louis, MO) binding experiments (50 mM Tris, 10 mM $MgCl_2$, 1 mM EDTA, pH 7.4). A Bradford protein assay (Bio-Rad, Hercules, CA) was used to determine the protein concentration. Membranes were used fresh for [^{3}H]-(*R*)-(+)-7-OH-DPAT binding experiments or diluted to 500 μg/mL and stored in a −80 °C freezer for later use in [^{3}H]*N*-methylspiperone binding experiments.

All test compounds were freshly dissolved in 30% dimethyl sulfoxide (DMSO) and 70% H_2O to a stock concentration of 100 μM. To assist the solubilization of free-base compounds, 10 μL of glacial acetic acid was added along with the DMSO. Each test compound was then diluted into half-log serial dilutions and tested in triplicate using the 30% DMSO vehicle. Competitive-inhibition experiments were conducted in 96-well plates containing 300 μL fresh binding buffer, 50 μL of diluted test compound, 100 μL of membrane suspension ([^{3}H]*N*-methylspiperone: 20 μg/well for D_2R and D_3R, 30 μg/well for D_4R; [^{3}H]-(*R*)-(+)-7-OH-DPAT: 80 μg/well for D_2R, 40 μg/well for D_3R, 60 μg/well for D_4R), and 50 μL of radioligand diluted in binding buffer ([^{3}H]*N*-methylspiperone: 0.4 nM final concentration for all receptors; [^{3}H]-(*R*)-(+)-7-OH-DPAT: 1.5 nM final concentration for D_2R, 0.5 nM final concentration for D_3R, 3 nM final concentration for D_4R). Aliquots of [^{3}H]*N*-methylspiperone and [^{3}H]-(*R*)-(+)-7-OH-DPAT solution were also quantified accurately to determine how much radioactivity was added. Nonspecific binding was determined using 10 μM (+)-butaclamol (Sigma-Aldrich, St. Louis, MO), and total binding was determined with 30% DMSO vehicle. The reaction was incubated for 60 ([^{3}H]*N*-methylspiperone) or 90 min ([^{3}H]-(*R*)-(+)-7-OH-DPAT) at room temperature and terminated by filtration through PerkinElmer UniFilter-96 GF/B plates, presoaked in 0.5% polyethylenimine, using a Brandel 96-well plate harvester manifold (Brandel Instruments, Gaithersburg, MD). Filters were washed three times (∼1 mL/well) with ice cold binding buffer. After drying, 65 μL PerkinElmer MicroScint 20 scintillation cocktail was added to each well and filters were counted after at least 18 h of incubation using a PerkinElmer MicroBeta Microplate Counter. IC_{50} values for each compound were determined from dose−response curves and K_i values were calculated using the Cheng−Prusoff equation in GraphPad Prism 6 (GraphPad Software, San Diego, CA).[50] K_d values for [^{3}H]*N*-methylspiperone and [^{3}H]-(*R*)-(+)-7-OH-DPAT were determined via separate homologous competitive binding experiments at each receptor. K_i values for each compound/receptor/radioligand combination were calculated from at least three independent experiments and are reported as means ± SEM.

Functional Assays. *β-Arrestin Recruitment Assay.* Assays were conducted with minor modifications as previously published by our laboratory,[31,51−54] using the DiscoverX PathHunter technology (DiscoverX, Inc., Fremont, CA). Briefly, CHO-K1 cells stably expressing the human D_2R long isoform, D_3R, or D_4R (DiscoverX, Inc.), were maintained in Ham's F12 media supplemented with 10% fetal bovine serum, 100 U/mL penicillin, 100 μg/mL streptomycin, and 800 μg/mL G418 and 300 μg/mL hygromycin at 37 °C, 5% CO_2, and 90% humidity. The cells were seeded in this media at a density of 2625 cells/well in 384-well black, clear-bottom plates. Compounds were diluted in phosphate-buffered saline in the presence of 0.2 μM sodium metabisulfite. Following overnight incubation, the cells were treated with multiple concentrations of compound and incubated at 37 °C for 90 min. DiscoverX reagent was then added to cells according to the manufacturer's recommendations followed by 45−60 min incubation at room temperature. Luminescence was measured on a Hamamatsu FDSS μCell reader. Data were collected as RLUs and subsequently normalized to a percentage of the control luminescence seen with a maximum concentration of dopamine for agonist mode assays and the EC_{80} of dopamine for antagonist mode assays. The Hill coefficients of the concentration−response curves did not significantly differ from unity.

cAMP Inhibition Assay. D_4R- and D_2R-mediated inhibition of forskolin-stimulated cAMP production was assayed using the PerkinElmer LANCE Ultra cAMP assay kit (PerkinElmer, Inc., Waltham, MA). CHO-K1 cells stably expressing the human D_2R long isoform or D_4R were maintained in Ham's F12 supplemented with 10% fetal bovine serum, 100 U/mL penicillin, 100 μg/mL streptomycin, and 800 μg/mL G418 and 300 μg/mL hygromycin at 37 °C, 5% CO_2, and 90% humidity. Cells were seeded in Hank's balanced salt solution (with CaCl and $MgCl_2$) with 5 mM HEPES buffer and 0.2 μM sodium metabisulfite at a density of 5000 cells/well in 384-well white plates. Compounds and forskolin were made in the same buffer. Immediately after plating, cells were treated with 2.5 μL of compound (at various concentrations) and 2.5 μL of forskolin and incubated at room temperature for 30 min. The final concentration of forskolin was 10 μM. When running assay in antagonist mode, the EC_{80} of dopamine (10 nM) was added with the forskolin solution. Eu-cAMP tracer and ULight-anti-cAMP solutions were added as directed by the manufacturer and cells were incubated for 2 h in the dark at room temperature, after which a time-resolved fluorescence resonance energy transfer (TR-FRET) signal was measured using a BMG Labtech PHERAstar Fs (BMG Labtech USA, Cary, NC). Values were normalized to a percentage of the control TR-FRET signal seen with a maximum concentration of dopamine for agonist mode assays and the EC_{80} of dopamine for antagonist mode assays. The Hill coefficients of the concentration−response curves did not significantly differ from unity with the data fitting to a single site model.

Molecular Docking Studies. *Crystal Structures of D_2R, D_3R, and D_4R.* In this study, we used the crystal structure of the human dopamine D_2, D_3, and D_4 receptor in complex with antagonists risperidone (PDB: 6CM4[26]), eticlopride (PDB: 3PBL[25]), and nemonapride (PDB: 5WIU[24]), respectively. Each of the three crystal structures was prealigned in membrane using the OPM web server.[55]

Protein Structure Preparation. The structures of D_2R, D_3R, and D_4R were further prepared using Maestro Protein Preparation Wizard.[56] First, the hydrogens and missing side chains were added. Second, the protonation state of the receptor was optimized at pH = 7. Third, a restrained minimization was performed to relax the receptor structure using OPLS3 force field.[57]

Ligand Preparation. The 2D structures of **1**, **6**, **9**, **10**, **12**, **13**, and **21** were first constructed in ChemDraw and then converted into a 3D structure using Maestro Elements. Next, the protonation state was generated at pH = 7 using the pK_a prediction program Epik that is based on the Hammett and Taft methodologies.[56] Lastly, the geometry of each ligand was optimized using an energy minimization.

Ligand Docking. The orthosteric ligand pockets of D_2R, D_3R, and D_4R were specified by the crystal ligands risperidone, eticlopride, and nemonapride, respectively, and a 3D box was formed around each crystal ligand to enclose the orthosteric ligand binding pocket. Each ligand was first docked using the Glide XP scoring function with default procedures and parameters.[58,59] Reproductions of the crystal binding poses of risperidone, eticlopride, and nemonapride in D_2R, D_3R, and D_4R, respectively, provide a solid validation for our XP docking protocol (Figures S2−S4). To refine the docking poses of

DOI: 10.1021/acs.jmedchem.9b00231
J. Med. Chem. 2019, 62, 3722−3740

noncrystal ligands, induced fit docking (IFD) was conducted on the complex from the Glide XP docking.

MD Simulation System Setup. Seven MD simulation systems were built using the complexes from the IFD. Each pre-aligned complex was placed in a double lipid membrane formed by 1-palmitoyl-2-oleoyl-*sn*-glycero-3-phosphocholine lipids[60] and then solvated in an orthorhombic water box with a buffer distance of 10 Å using the SPC water model.[61] Each system was neutralized using Na^+ ions, added with a salt concentration of 0.15 M NaCl. The OPLS3 force field[57] was used to represent the receptor−ligand−lipid system.

Relaxation and Production Runs. Using Desmond, each system was first relaxed using the default relaxation protocol for membrane proteins.[62] After the relaxation, a 100.0 ns production run was conducted under the *NPT* ensemble for each system using the default protocol. A temperature of 300 K was controlled using the Nosé−Hoover chain coupling scheme[63] with a coupling constant of 1.0 ps. A pressure of 1 atm was controlled using the Martyna−Tuckerman−Klein chain coupling scheme[63] with a coupling constant of 2.0 ps. M-SHAKE[64] was applied to constrain all bonds connecting hydrogen atoms, enabling a 2.0 fs time step in the simulations. The *k*-space Gaussian split Ewald method[65] was used to treat long-range electrostatic interactions under periodic boundary conditions (charge grid spacing of ∼1.0 Å, and direct sum tolerance of 10^{-9}). The cutoff distance for short-range nonbonded interactions was 9 Å, with the long-range van der Waals interactions based on a uniform density approximation. To reduce the computation, nonbonded forces were calculated using an r-RESPA integrator[66] where the short-range forces were updated every step and the long-range forces were updated every three steps. The trajectories were saved at 100.0 ps intervals for analysis.

SID Analyses. The SID tool was used to generate graphical information about the behavior and interaction of the protein and ligand during simulation. The analysis gives us graphical representation of root mean square deviation (RMSD), root mean square fluctuation, secondary structures changes, protein−ligand contacts, and ligand torsion profiles of rotatable bonds.

Convergence of Simulations. To check the convergence of the simulations, we investigated the protein Cα and ligand RMSD plots for each system (Figures S34−S36). The relatively flat plots within last 20 ns indicate that the complex systems have reached a steady state.

Trajectory Clustering Analyses. The Desmond trajectory clustering tool[67] was used to group complex structures for each system. The backbone RMSD matrix was used as structural similarity metric and hierarchical clustering with average linkage[67] was selected as the clustering method. The merging distance cutoff was set to be 2.5 Å. For all systems, a dominant cluster with was identified to have more than 80% of the trajectory population.

■ ASSOCIATED CONTENT

Supporting Information

The Supporting Information is available free of charge on the ACS Publications website at DOI: 10.1021/acs.jmedchem.9b00231.

Representation of compound effects on D_1-like dopamine receptors and comparison of ligand−residue contacts in the D_2-like receptors; list of MD simulations and the examples of validation analysis; and elemental analysis for all final compounds results and liquid chromatography/mass spectrometry data for compound **9** (PDF)

SMILES data (CSV)

■ AUTHOR INFORMATION

Corresponding Author

*E-mail: cboateng@highpoint.edu. Phone: (336)-841-9718. Fax: (336)-888-6394.

ORCID

Thomas M. Keck: 0000-0003-1845-9373

Amy H. Newman: 0000-0001-9065-4072

Comfort A. Boateng: 0000-0003-1907-431X

Author Contributions

#T.M.K., R.B.F., and C.A.B. are equally contributing authors.

Notes

The authors declare no competing financial interest.

■ ACKNOWLEDGMENTS

Support for this research was provided by High Point University, Fred Wilson School of Pharmacy. Additional support was provided by the National Institute of Neurological Disorders and Stroke-Intramural Research Program, National Institute on Drug Abuse-Intramural Research Program (Z1A DA000609), and Rowan University. We acknowledge the technical assistance of Megan Donegan, Peace Nwankwo, and Allison Engle.

■ ABBREVIATIONS

TM, transmembrane; D_2R, dopamine D_2 receptor; D_3R, dopamine D_3 receptor; D_4R, dopamine D_4 receptor; $CDCl_3$, deuterated chloroform; D_2O, deuterium oxide; EtOAc, ethyl acetate; PP, phenylpiperazine

■ REFERENCES

(1) Beaulieu, J.-M.; Gainetdinov, R. R. The physiology, signaling, and pharmacology of dopamine receptors. *Pharmacol. Rev.* **2011**, *63*, 182−217.

(2) González, S.; Rangel-Barajas, C.; Peper, M.; Lorenzo, R.; Moreno, E.; Ciruela, F.; Borycz, J.; Ortiz, J.; Lluís, C.; Franco, R.; McCormick, P. J.; Volkow, N. D.; Rubinstein, M.; Floran, B.; Ferré, S. Dopamine D4 receptor, but not the ADHD-associated D4.7 variant, forms functional heteromers with the dopamine D2S receptor in the brain. *Mol. Psychiatr.* **2012**, *17*, 650−662.

(3) Oak, J. N.; Oldenhof, J.; Van Tol, H. H. M. The dopamine D4 receptor: one decade of research. *Eur. J. Pharmacol.* **2000**, *405*, 303−327.

(4) Powell, S.; Paulus, M. P.; Hartman, D. S.; Godel, T.; Geyer, M. A. RO-10-5824 is a selective dopamine D4 receptor agonist that increases novel object exploration in C57 mice. *Neuropharmacology* **2003**, *44*, 473−481.

(5) Woolley, M. L.; Waters, K. A.; Reavill, C.; Bull, S.; Lacroix, L. P.; Martyn, A. J.; Hutcheson, D. M.; Valerio, E.; Bate, S.; Jones, D. N. C.; Dawson, L. A. Selective dopamine D4 receptor agonist (A-412997) improves cognitive performance and stimulates motor activity without influencing reward-related behaviour in rat. *Behav. Pharmacol.* **2008**, *19*, 765−776.

(6) Bernaerts, P.; Tirelli, E. Facilitatory effect of the dopamine D4 receptor agonist PD168,077 on memory consolidation of an inhibitory avoidance learned response in C57BL/6J mice. *Behav. Brain Res.* **2003**, *142*, 41−52.

(7) Huang, M.; Kwon, S.; He, W.; Meltzer, H. Y. Neurochemical arguments for the use of dopamine D 4 receptor stimulation to improve cognitive impairment associated with schizophrenia. *Pharmacol., Biochem. Behav.* **2017**, *157*, 16−23.

(8) Miyauchi, M.; Neugebauer, N. M.; Meltzer, H. Y. Dopamine D4 receptor stimulation contributes to novel object recognition: Relevance to cognitive impairment in schizophrenia. *J. Psychopharmacol.* **2017**, *31*, 442−452.

(9) Andersson, R. H.; Johnston, A.; Herman, P. A.; Winzer-Serhan, U. H.; Karavanova, I.; Vullhorst, D.; Fisahn, A.; Buonanno, A. Neuregulin and dopamine modulation of hippocampal gamma oscillations is dependent on dopamine D4 receptors. *Proc. Natl. Acad. Sci. U.S.A.* **2012**, *109*, 13118−13123.

DOI: 10.1021/acs.jmedchem.9b00231
J. Med. Chem. 2019, 62, 3722−3740

(10) Rondou, P.; Haegeman, G.; Van Craenenbroeck, K. The dopamine D4 receptor: Biochemical and signalling properties. *Cell. Mol. Life Sci.* **2010**, *67*, 1971−1986.

(11) Tomlinson, A.; Grayson, B.; Marsh, S.; Hayward, A.; Marshall, K. M.; Neill, J. C. Putative therapeutic targets for symptom subtypes of adult ADHD: D4 receptor agonism and COMT inhibition improve attention and response inhibition in a novel translational animal model. *Eur. Neuropsychopharmacol.* **2015**, *25*, 454−467.

(12) Negrete-Diaz, J. V.; Shumilov, K.; Real, M. A.; Medina-Luque, J.; Valderrama-Carvajal, A.; Flores, G.; Rodriguez-Moreno, A.; Rivera, A. Pharmacological activation of dopamine D4 receptor modulates morphine-induced changes in the expression of GAD65/67 and GABAB receptors in the basal ganglia. *Neuropharmacology* **2019**, DOI: 10.1016/j.neuropharm.2019.01.024.

(13) Rivera, A.; Gago, B.; Suárez-Boomgaard, D.; Yoshitake, T.; Roales-Buján, R.; Valderrama-Carvajal, A.; Bilbao, A.; Medina-Luque, J.; Díaz-Cabiale, Z.; Craenenbroeck, K. V.; Borroto-Escuela, D. O.; Kehr, J.; Rodríguez de Fonseca, F.; Santín, L.; de la Calle, A.; Fuxe, K. Dopamine D4 receptor stimulation prevents nigrostriatal dopamine pathway activation by morphine: relevance for drug addiction. *Addict. Biol.* **2017**, *22*, 1232−1245.

(14) Di Ciano, P.; Grandy, D. K.; Le Foll, B. Dopamine D4 receptors in psychostimulant addiction. *Adv. Pharmacol.* **2014**, *69*, 301−321.

(15) Lauzon, N. M.; Laviolette, S. R. Dopamine D4-receptor modulation of cortical neuronal network activity and emotional processing: Implications for neuropsychiatric disorders. *Behav. Brain Res.* **2010**, *208*, 12−22.

(16) Bergman, J.; Rheingold, C. Dopamine D4 receptor antagonists for the treatment of cocaine use disorders. *CNS Neurol. Disord.: Drug Targets* **2015**, *14*, 707−715.

(17) Lindsley, C. W.; Hopkins, C. R. Return of D4 Dopamine Receptor Antagonists in Drug Discovery. *J. Med. Chem.* **2017**, *60*, 7233−7243.

(18) Huot, P.; Johnston, T. H.; Koprich, J. B.; Aman, A.; Fox, S. H.; Brotchie, J. M. L-745,870 reduces L-DOPA-induced dyskinesia in the 1-methyl-4-phenyl-1,2,3,6-tetrahydropyridine-lesioned macaque model of Parkinson's disease. *J. Pharmacol. Exp. Ther.* **2012**, *342*, 576−585.

(19) Hisahara, S.; Shimohama, S. Dopamine receptors and Parkinson's disease. *Int. J. Med. Chem.* **2011**, *2011*, 403039.

(20) Sebastianutto, I.; Maslava, N.; Hopkins, C. R.; Cenci, M. A. Validation of an improved scale for rating l-DOPA-induced dyskinesia in the mouse and effects of specific dopamine receptor antagonists. *Neurobiol. Dis.* **2016**, *96*, 156−170.

(21) Moreland, R. B.; Patel, M.; Hsieh, G. C.; Wetter, J. M.; Marsh, K.; Brioni, J. D. A-412997 is a selective dopamine D4 receptor agonist in rats. *Pharmacol., Biochem. Behav.* **2005**, *82*, 140−147.

(22) Patel, M. V.; Kolasa, T.; Mortell, K.; Matulenko, M. A.; Hakeem, A. A.; Rohde, J. J.; Nelson, S. L.; Cowart, M. D.; Nakane, M.; Miller, L. N.; Uchic, M. E.; Terranova, M. A.; El-Kouhen, O. F.; Donnelly-Roberts, D. L.; Namovic, M. T.; Hollingsworth, P. R.; Chang, R.; Martino, B. R.; Wetter, J. M.; Marsh, K. C.; Martin, R.; Darbyshire, J. F.; Gintant, G.; Hsieh, G. C.; Moreland, R. B.; Sullivan, J. P.; Brioni, J. D.; Stewart, A. O. Discovery of 3-Methyl-N-(1-oxy-3′,4′,5′,6′-tetrahydro-2′H-[2,4′-bipyridine]-1′-ylmethyl)benzamide (ABT-670), an Orally Bioavailable Dopamine D4Agonist for the Treatment of Erectile Dysfunction. *J. Med. Chem.* **2006**, *49*, 7450−7465.

(23) Browman, K. E.; Curzon, P.; Pan, J. B.; Molesky, A. L.; Komater, V. A.; Decker, M. W.; Brioni, J. D.; Moreland, R. B.; Fox, G. B. A-412997, a selective dopamine D4 agonist, improves cognitive performance in rats. *Pharmacol., Biochem. Behav.* **2005**, *82*, 148−155.

(24) Wang, S.; Wacker, D.; Levit, A.; Che, T.; Betz, R. M.; McCorvy, J. D.; Venkatakrishnan, A. J.; Huang, X.-P.; Dror, R. O.; Shoichet, B. K.; Roth, B. L. D4dopamine receptor high-resolution structures enable the discovery of selective agonists. *Science* **2017**, *358*, 381−386.

(25) Chien, E. Y. T.; Liu, W.; Zhao, Q.; Katritch, V.; Won Han, G.; Hanson, M. A.; Shi, L.; Newman, A. H.; Javitch, J. A.; Cherezov, V.; Stevens, R. C. Structure of the human dopamine D3 receptor in complex with a D2/D3 selective antagonist. *Science* **2010**, *330*, 1091−1095.

(26) Wang, S.; Che, T.; Levit, A.; Shoichet, B. K.; Wacker, D.; Roth, B. L. Structure of the D2 dopamine receptor bound to the atypical antipsychotic drug risperidone. *Nature* **2018**, *555*, 269−273.

(27) Matulenko, M. A.; Hakeem, A. A.; Kolasa, T.; Nakane, M.; Terranova, M. A.; Uchic, M. E.; Miller, L. N.; Chang, R.; Donnelly-Roberts, D. L.; Namovic, M. T.; Moreland, R. B.; Brioni, J. D.; Stewart, A. O. Synthesis and functional activity of (2-aryl-1-piperazinyl)-N-(3-methylphenyl)acetamides: Selective dopamine D4 receptor agonists. *Bioorg. Med. Chem.* **2004**, *12*, 3471−3483.

(28) Sampson, D.; Zhu, X. Y.; Eyunni, S. V. K.; Etukala, J. R.; Ofori, E.; Bricker, B.; Lamango, N. S.; Setola, V.; Roth, B. L.; Ablordeppey, S. Y. Identification of a new selective dopamine D4 receptor ligand. *Bioorg. Med. Chem.* **2014**, *22*, 3105−3114.

(29) Boateng, C. A.; Bakare, O. M.; Zhan, J.; Banala, A. K.; Burzynski, C.; Pommier, E.; Keck, T. M.; Donthamsetti, P.; Javitch, J. A.; Rais, R.; Slusher, B. S.; Xi, Z.-X.; Newman, A. H. High affinity dopamine D3 receptor (D3R)-selective antagonists attenuate heroin self-administration in wild-type but not D3R knockout mice. *J. Med. Chem.* **2015**, *58*, 6195−6213.

(30) Zou, M.-F.; Keck, T. M.; Kumar, V.; Donthamsetti, P.; Michino, M.; Burzynski, C.; Schweppe, C.; Bonifazi, A.; Free, R. B.; Sibley, D. R.; Janowsky, A.; Shi, L.; Javitch, J. A.; Newman, A. H. Novel analogues of (R)-5-(Methylamino)-5,6-dihydro-4H-imidazo-[4,5,1-ij]quinolin-2(1H)-one (Sumanirole) provide clues to dopamine D2/D3 receptor agonist selectivity. *J. Med. Chem.* **2016**, *59*, 2973−2988.

(31) Banala, A. K.; Levy, B. A.; Khatri, S. S.; Furman, C. A.; Roof, R. A.; Mishra, Y.; Griffin, S. A.; Sibley, D. R.; Luedtke, R. R.; Newman, A. H. N-(3-fluoro-4-(4-(2-methoxy or 2,3-dichlorophenyl)piperazine-1-yl)butyl)arylcarboxamides as selective dopamine D3 receptor ligands: critical role of the carboxamide linker for D3 receptor selectivity. *J. Med. Chem.* **2011**, *54*, 3581−3594.

(32) van Rhee, A. M.; Jacobson, K. A. Molecular architecture of G protein-coupled receptors. *Drug Dev. Res.* **1996**, *37*, 1−38.

(33) Stewart, A. O.; Cowart, M. D.; Moreland, R. B.; Latshaw, S. P.; Matulenko, M. A.; Bhatia, P. A.; Wang, X.; Daanen, J. F.; Nelson, S. L.; Terranova, M. A.; Namovic, M. T.; Donnelly-Roberts, D. L.; Miller, L. N.; Nakane, M.; Sullivan, J. P.; Brioni, J. D. Dopamine D4Ligands and Models of Receptor Activation: 2-(4-Pyridin-2-ylpiperazin-1-ylmethyl)-1H-benzimidazole and Related Heteroaryl-methylarylpiperazines Exhibit a Substituent Effect Responsible for Additional Efficacy Tuning. *J. Med. Chem.* **2004**, *47*, 2348−2355.

(34) Löber, S.; Hübner, H.; Utz, W.; Gmeiner, P. Rationally Based Efficacy Tuning of Selective Dopamine D4 Receptor Ligands Leading to the Complete Antagonist 2-[4-(4-Chlorophenyl)piperazin-1-ylmethyl]pyrazolo[1,5-a]pyridine (FAUC 213). *J. Med. Chem.* **2001**, *44*, 2691−2694.

(35) Helms, C. M.; Gubner, N. R.; Wilhelm, C. J.; Mitchell, S. H.; Grandy, D. K. D4 receptor deficiency in mice has limited effects on impulsivity and novelty seeking. *Pharmacol., Biochem. Behav.* **2008**, *90*, 387−393.

(36) Dulawa, S. C.; Grandy, D. K.; Low, M. J.; Paulus, M. P.; Geyer, M. A. Dopamine D4 receptor-knock-out mice exhibit reduced exploration of novel stimuli. *J. Neurosci.* **1999**, *19*, 9550−9556.

(37) Benjamin, J.; Li, L.; Patterson, C.; Greenberg, B. D.; Murphy, D. L.; Hamer, D. H. Population and familial association between the D4 dopamine receptor gene and measures of novelty seeking. *Nat. Genet.* **1996**, *12*, 81−84.

(38) Bailey, J. N.; Breidenthal, S. E.; Jorgensen, M. J.; McCracken, J. T.; Fairbanks, L. A. The association of DRD4 and novelty seeking is found in a nonhuman primate model. *Psychiatr. Genet.* **2007**, *17*, 23−27.

(39) Falzone, T. L.; Gelman, D. M.; Young, J. I.; Grandy, D. K.; Low, M. J.; Rubinstein, M. Absence of dopamine D4 receptors results in enhanced reactivity to unconditioned, but not conditioned, fear. *Eur. J. Neurosci.* **2002**, *15*, 158−164.

DOI: 10.1021/acs.jmedchem.9b00231
J. Med. Chem. 2019, 62, 3722−3740

(40) Keck, T. M.; Suchland, K. L.; Jimenez, C. C.; Grandy, D. K. Dopamine D4 receptor deficiency in mice alters behavioral responses to anxiogenic stimuli and the psychostimulant methylphenidate. *Pharmacol., Biochem. Behav.* **2013**, *103*, 831−841.

(41) Hutchinson, K. E.; McGeary, J.; Smolen, A.; Bryan, A.; Swift, R. M. The DRD4 VNTR polymorphism moderates craving after alcohol consumption. *Health Psychol.* **2002**, *21*, 139−146.

(42) Feldpausch, D. L.; Needham, L. M.; Stone, M. P.; Althaus, J. S.; Yamamoto, B. K.; Svensson, K. A.; Merchant, K. M. The role of dopamine D4 receptor in the induction of behavioral sensitization to amphetamine and accompanying biochemical and molecular adaptations. *J. Pharmacol. Exp. Ther.* **1998**, *286*, 497−508.

(43) Kruzich, P. J.; Suchland, K. L.; Grandy, D. K. Dopamine D4 receptor-deficient mice, congenic on the C57BL/6J background, are hypersensitive to amphetamine. *Synapse* **2004**, *53*, 131−139.

(44) Svingos, A. L.; Periasamy, S.; Pickel, V. M. Presynaptic dopamine D4 receptor localization in the rat nucleus accumbens shell. *Synapse* **2000**, *36*, 222−232.

(45) Good, C. H.; Wang, H.; Chen, Y.-H.; Mejias-Aponte, C. A.; Hoffman, A. F.; Lupica, C. R. Dopamine D4Receptor Excitation of Lateral Habenula Neurons via Multiple Cellular Mechanisms. *J. Neurosci.* **2013**, *33*, 16853−16864.

(46) Root, D. H.; Hoffman, A. F.; Good, C. H.; Zhang, S.; Gigante, E.; Lupica, C. R.; Morales, M. Norepinephrine activates dopamine D4 receptors in the rat lateral habenula. *J. Neurosci.* **2015**, *35*, 3460−3469.

(47) Sanchez-Soto, M.; Bonifazi, A.; Cai, N. S.; Ellenberger, M. P.; Newman, A. H.; Ferre, S.; Yano, H. Evidence for noncanonical neurotransmitter activation: Norepinephrine as a dopamine D2-like receptor agonist. *Mol. Pharmacol.* **2016**, *89*, 457−466.

(48) Del Bello, F.; Bonifazi, A.; Giorgioni, G.; Cifani, C.; Micioni Di Bonaventura, M. V.; Petrelli, R.; Piergentili, A.; Fontana, S.; Mammoli, V.; Yano, H.; Matucci, R.; Vistoli, G.; Quaglia, W. 1-[3-(4-Butylpiperidin-1-yl)propyl]-1,2,3,4-tetrahydroquinolin-2-one (77-LH-28-1) as a model for the rational design of a novel class of brain penetrant ligands with high affinity and selectivity for dopamine D4 receptor. *J. Med. Chem.* **2018**, *61*, 3712−3725.

(49) Bhatia, P. A.; Daanen, J. F.; Hakeem, A. A.; Kolasa, T.; Matulenko, M. A.; Mortell, K.; Patel, M.; Stewart, A. O.; Wang, X.; Xia, Z.; Zhang, H. Acetamides and Benzamides that are Useful in Treating Sexual Dysfunction. U.S. Patent 7,528,134, May 5, 2009.

(50) Yung-Chi, C.; Prusoff, W. H. Relationship between the inhibition constant (K_1) and the concentration of inhibitor which causes 50 per cent inhibition (I_{50}) of an enzymatic reaction. *Biochem. Pharmacol.* **1973**, *22*, 3099−3108.

(51) Bergman, J.; Roof, R. A.; Furman, C. A.; Conroy, J. L.; Mello, N. K.; Sibley, D. R.; Skolnick, P. Modification of cocaine self-administration by buspirone (buspar): potential involvement of D3 and D4 dopamine receptors. *Int. J. Neuropsychopharmacol.* **2013**, *16*, 445−458.

(52) Free, R. B.; Chun, L. S.; Moritz, A. E.; Miller, B. N.; Doyle, T. B.; Conroy, J. L.; Padron, A.; Meade, J. A.; Xiao, J.; Hu, X.; Dulcey, A. E.; Han, Y.; Duan, L.; Titus, S.; Bryant-Genevier, M.; Barnaeva, E.; Ferrer, M.; Javitch, J. A.; Beuming, T.; Shi, L.; Southall, N. T.; Marugan, J. J.; Sibley, D. R. Discovery and Characterization of a G Protein-Biased Agonist That Inhibits -Arrestin Recruitment to the D2 Dopamine Receptor. *Mol. Pharmacol.* **2014**, *86*, 96−105.

(53) Meade, J. A.; Free, R. B.; Miller, N. R.; Chun, L. S.; Doyle, T. B.; Moritz, A. E.; Conroy, J. L.; Watts, V. J.; Sibley, D. R. (-)-Stepholidine is a potent pan-dopamine receptor antagonist of both G protein- and β-arrestin-mediated signaling. *Psychopharmacology* **2015**, *232*, 917−930.

(54) Chun, L. S.; Vekariya, R. H.; Free, R. B.; Li, Y.; Lin, D. T.; Su, P.; Liu, F.; Namkung, Y.; Laporte, S. A.; Moritz, A. E.; Aube, J.; Frankowski, K. J.; Sibley, D. R. Structure-activity investigation of a G protein-biased agonist reveals molecular determinants for biased signaling of the D2 dopamine receptor. *Front. Synaptic Neurosci.* **2018**, *10*, 2.

(55) Lomize, M. A.; Pogozheva, I. D.; Joo, H.; Mosberg, H. I.; Lomize, A. L. OPM database and PPM web server: resources for positioning of proteins in membranes. *Nucleic Acids Res.* **2012**, *40*, D370−D376.

(56) Sastry, G. M.; Adzhigirey, M.; Day, T.; Annabhimoju, R.; Sherman, W. Protein and ligand preparation: parameters, protocols, and influence on virtual screening enrichments. *J. Comput. Aided Mol. Des.* **2013**, *27*, 221−234.

(57) Harder, E.; Damm, W.; Maple, J.; Wu, C.; Reboul, M.; Xiang, J. Y.; Wang, L.; Lupyan, D.; Dahlgren, M. K.; Knight, J. L.; Kaus, J. W.; Cerutti, D. S.; Krilov, G.; Jorgensen, W. L.; Abel, R.; Friesner, R. A. OPLS3: A force field providing broad coverage of drug-like small molecules and proteins. *J. Chem. Theory Comput.* **2016**, *12*, 281−296.

(58) Friesner, R. A.; Banks, J. L.; Murphy, R. B.; Halgren, T. A.; Klicic, J. J.; Mainz, D. T.; Repasky, M. P.; Knoll, E. H.; Shelley, M.; Perry, J. K.; Shaw, D. E.; Francis, P.; Shenkin, P. S. Glide: a new approach for rapid, accurate docking and scoring. 1. Method and assessment of docking accuracy. *J. Med. Chem.* **2004**, *47*, 1739−1749.

(59) Friesner, R. A.; Murphy, R. B.; Repasky, M. P.; Frye, L. L.; Greenwood, J. R.; Halgren, T. A.; Sanschagrin, P. C.; Mainz, D. T. Extra Precision Glide: Docking and Scoring Incorporating a Model of Hydrophobic Enclosure for Protein−Ligand Complexes. *J. Med. Chem.* **2006**, *49*, 6177−6196.

(60) Lyman, E.; Higgs, C.; Kim, B.; Lupyan, D.; Shelley, J. C.; Farid, R.; Voth, G. A. A Role for a Specific Cholesterol Interaction in Stabilizing the Apo Configuration of the Human A 2A Adenosine Receptor. *Structure* **2009**, *17*, 1660−1668.

(61) Mark, P.; Nilsson, L. Structure and Dynamics of the TIP3P, SPC, and SPC/E Water Models at 298 K. *J. Phys. Chem. A* **2001**, *105*, 9954−9960.

(62) Zhang, J.; Hou, Y.; Wang, Y.; Wang, C.; Zhang, X. The LBFGS quasi-Newtonian method for molecular modeling prion AGAAAAGA amyloid fibrils. *Nat. Sci.* **2012**, *04*, 1097−1108.

(63) Ikeguchi, M. Partial rigid-body dynamics in NPT, NPAT and NP?T ensembles for proteins and membranes. *J. Comput. Chem.* **2004**, *25*, 529−541.

(64) Bailey, A. G.; Lowe, C. P. MILCH SHAKE: an efficient method for constraint dynamics applied to alkanes. *J. Comput. Chem.* **2009**, *30*, 2485−2493.

(65) Shan, Y.; Klepeis, J. L.; Eastwood, M. P.; Dror, R. O.; Shaw, D. E. Gaussian split Ewald: A fast Ewald mesh method for molecular simulation. *J. Chem. Phys.* **2005**, *122*, 054101.

(66) Stuart, S. J.; Zhou, R.; Berne, B. J. Molecular dynamics with multiple time scales: The selection of efficient reference system propagators. *J. Chem. Phys.* **1996**, *105*, 1426−1436.

(67) Bowers, K. J.; Sacerdoti, F. D.; Salmon, J. K.; Shan, Y.; Shaw, D. E.; Chow, E.; Xu, H.; Dror, R. O.; Eastwood, M. P.; Gregersen, B. A.; Klepeis, J. L.; Kolossvary, I.; Moraes, M. A. Scalable algorithms for molecular dynamics simulations on commodity clusters. *Proceedings of the 2006 ACM/IEEE Conference on Supercomputing*, 2006; Article no. 84.

DOI: 10.1021/acs.jmedchem.9b00231
J. Med. Chem. 2019, 62, 3722−3740